Dynamics of transcription factor and histone modification in activity-dependent gene expression in human cortical neurons

ヒト大脳皮質神経細胞の神経活動依存的な遺伝子発現における転写調節因子の動態変化とヒストン修飾

大阪大学大学院 生命機能研究科

渥美　友梨

令和 6 年 3 月修了

Dynamics of transcription factor and histone modification in activity-dependent gene expression in human cortical neurons

Yuri Atsumi

KOKORO-Biology Group (Yagi Lab.)

Graduate School of Frontier Biosciences, Osaka University Suita, Osaka

March, 2024

Summary

Neuronal activity-dependent transcription plays a key role in plasticity and pathology in the brain. An intriguing question is how neuronal activity controls gene expression via interactions of transcription factors with DNA and chromatin modifiers in the nucleus. By utilizing single-molecule imaging in human embryonic stem cell (ESC)-derived cortical neurons, I demonstrated that neuronal activity increased repetitive emergence of cAMP response element-binding protein (CREB) at histone acetylation sites in the nucleus, where RNA polymerase II (RNAPII) accumulation and FOS and NR4A1 expression occurred rapidly. Neuronal activity also enhanced co-localization of CREB and CREB-binding protein (CBP). Increased binding of a constitutively active CREB to CBP efficiently induced CREB repetitive emergence. On the other hand, the formation of histone acetylation sites was dependent on CBP histone modification via acetyltransferase (HAT) activity but was not affected by neuronal activity. Taken together, these results suggest that neuronal activity promotes repetitive CREB-CRE and CREB-CBP interactions at predetermined histone acetylation sites, leading to rapid gene expression.

Contents

General Introduction

The brain is a huge network composed of about 100 billion neurons, which underlies complex behavior and thought. How is the network, neuronal wiring, formed? During the development, intrinsic programs and extrinsic environmental factors contribute to the formation and remodeling of neuronal circuits. The intrinsic programs may control the expression of the guidance molecules in predetermined regions and timings contribute to formation of fundamental neuronal circuits at early developmental stages. For example, Netrin1/Dcc and Slit/Robo1 expressed in specific cell populations in the spinal cord control commissural axon guidance (Serafini et al., 1996; Fazeli et al., 1997; Bagri et al., 2002; Andrews et al., 2006). EphrinA/EphA expressed in the cortical layers 2/3 and 5 where most of the callosal neurons, is required for midline crossing of corpus callosum (Hu et al., 2003; Nishikimi et al., 2013). However, these intrinsic programs are not sufficient for building up the functional neuronal circuits.

Sensory-evoked activity elicited by extrinsic environmental stimuli modifies neuronal connections. The ocular dominance (OD) column in the visual cortex is a well-known model to investigate how visual inputs are important in neuronal circuit formation (Hubel and Wiesel, 1962). In mammals with binocular vision such as cats, monkeys and humans, geniculocortical axons serving left and right eyes are segregated in the visual cortex and form the functional columns (Hubel and Wiesel, 1968; Adams et al., 2007). However, the occlusion of one eye in kitten decreases geniculocortical projection serving the closed eye, and

conversely increases geniculocortical projection serving the open eye (Wiesel and Hubel, 1963; Hubel and Wiesel, 1970; Antonini and Stryker, 1993, 1996). Rodent barrel cortex is also known as another well-characterized model. In the somatosensory cortex in mice and rats, layer IV neurons form cylindrical aggregates named “barrels” which are innervated by thalamocortical axons and replicate the patterned array of whiskers on the contralateral snout (Woolsey and Van der Loos, 1970; Erzurumlu and Gaspar, 2012). Blocking sensory input by giving a damage to whisker follicle disrupts the whisker-specific pattern (Van der Loos and Woolsey, 1973; Harris and Woolsey, 1981). Thus, sensory-evoked activity plays an important role in establishing complex neuronal circuits.

In addition to sensory-evoked activity, neuronal activity spontaneously generated in various parts of nervous system such as cerebral cortex, cerebellum, hippocampus and retina is also involved in neuronal remodeling before sensory inputs (Latham and Paul, 1971; Flint et al., 1999; Yamamoto and López-Bendito, 2012). In the retina, patterned spontaneous activity called retinal waves appeared before eye opening (Butts et al., 1999). Blocking retinal waves during the embryonic stages prevents the segregation of retinal ganglion cell (RGC) axons projecting to the lateral geniculate nucleus (LGN) (Shatz and Stryker, 1988; Torborg and Feller, 2005). Moreover, an in vitro study showed that spontaneous activity can promote thalamocortical (TC) axon branching (Uesaka et al., 2007).

Activity-dependent gene expression in response to elevation of sensory-evoked and spontaneous activity is the molecular bases that neuronal activity

modifies neuronal circuit. So far, it has been reported that neuronal activity stimulates the transcription of several hundreds of activity-dependent genes with different time courses and magnitudes of induction (Flavell and Greenberg, 2008; Tyssowski et al., 2018). A large population of activity-dependent genes are effector molecules that regulate axon growth, branch formation and synapse formation directly. In excitatory neurons of cerebral cortex, hippocampus and striatum, brain-derived neurotrophic factor (BDNF) released from dendrites and cell bodies regulates axon and dendritic growth and synapse formation by binding to TrkB receptors (McAllister et al., 1996; Horch and Katz, 2002; Greer and Greenberg, 2008; Granseth et al., 2013; Park and Poo, 2013). Activity-regulated cytoskeleton-associated protein (Arc) is localized in post synapses of excitatory neurons, and acts in the final stages of synapse elimination in Purkinje cells and hippocampal CA1 neurons by removing synapses around cell bodies (Mikuni et al., 2013; Wilkerson et al., 2014). Netrin-4 is highly expressed in the developing cortex in response to neuronal activity, and promotes thalamocortical axon branching (Hayano et al., 2014). Furthermore, Robo1 whose expression is silenced by the spontaneous activity negatively regulates axon growth and extension into the cortex (Mire et al., 2012).

How does neuronal activity regulate expression of the effector molecules that alter synaptic remodeling? First, neuronal activity induces calcium influx to the nucleus through the N-methyl-D-aspartate type (NMDA) glutamate receptors and L-type voltage-sensitive calcium channels (VSCCs), and the calcium signals subsequently activates multiple signaling pathways such as Ras/MAP

and CaM kinase signaling to turn on the transcription through binding of transcription factors to enhancers and promoters (Greer and Greenberg, 2008; Fowler et al., 2011). Among such transcription factors, cAMP response element binding protein (CREB) is an essential transcription factors for the transcription of activity-dependent genes. CREB activates the expression of transcriptional regulators such as FOS, EGR1 and NPAS4, and these transcriptional regulators subsequently induce the expression of effector molecules such as BDNF and ARC (Lee and Fields, 2021). Neuronal activity induces rapid phosphorylation of CREB on Ser133 and its binding to cAMP-response element (CRE) sequences, and initiates transcription accompanied by RNA polymerase II (RNAPII) recruitment (Mayr and Montminy, 2001; Lonze and Ginty, 2002; Greer and Greenberg, 2008). Previous studies with transgenic mice suggest that CREB positively regulates memory consolidation and affects memory performance (Suzuki et al., 2011; Morè et al., 2022).

Furthermore, epigenetic regulation is also involved in the regulation of activity-dependent gene expression. Epigenetic changes affect gene expression positively and negatively but do not alter DNA sequences. In general, epigenetic regulation is classified into DNA methylation that blocks gene expression by attaching methyl groups directly to DNA, and histone modifications (histone acetylation, methylation and ubiquitination) that change chromatin structure. In fact, CREB binding to CRE sequence remarkably is known to be decreased by DNA methylation (Mancini et al., 1999; Zhang et al., 2005). In addition, H3K27me3 is involved in the transcriptional repression and inactive genes via

chromatin condensation (Kim et al., 2010). Conversely, H3K27ac and H3K4me1 accumulate in promoters and enhancers of activity-dependent genes, and the accumulation of these histone marks relaxes chromatin structure and contributes to the transcriptional activation (Kim et al., 2010; Malik et al., 2014; Kim et al., 2021). In particular, CREB binding protein (CBP), a coactivator of CREB, has histone acetyltransferase (HAT) activity, suggesting that histone acetylation is deeply involved in CREB-dependent transcriptional activation (Bannister and Kouzarides, 1996). Thus, previous studies have demonstrated the fundamental molecular mechanisms of activity-dependent gene expression. However, the interactions between transcription factors and DNA or epigenetic factors are not fully uncovered.

Co-immunoprecipitation (Co-IP) and chromatin immunoprecipitation (ChIP) have been used to detect molecular binding to DNA and other molecules, but these end point assays are analyses at the cell population level and have limited temporal resolution. Although fluorescence recovery after photobleaching (FRAP) is a method to explain molecular interaction and diffusion by observing the dynamics of proteins including transcriptional regulators in living cells, it is not able to track individual proteins and it is difficult to quantify the dynamics of proteins with short binding times (Mueller et al., 2010; Mazza et al., 2012). To overcome these problems, single-molecule imaging technique has been developed, which can track a single protein labelled by a fluorescence protein. Single-molecule imaging allows detailed spatiotemporal analysis of proteins with short residence times, minor

subpopulations, and the order of multistep molecular bindings (Liu and Tjian, 2018). Speil et al. succeeded in the observation of transcription factor STAT1 dynamics in HeLa cells at the single-molecule level (Speil et al., 2011), followed by several studies in single-molecule visualization of other transcription factors such as Sox2 and Oct4 (Specht et al., 2013; Chen et al., 2014; Liu et al., 2014; Hipp et al., 2019; Okamoto et al., 2023). These studies revealed that a small fraction of transcription factors bound at their binding sites, and that the binding time was on the order of seconds (Sugo et al., 2015; de Jonge et al., 2022). Thus, single-molecule imaging is suitable for investigating a small population of transcription factor dynamics with short binding times, and can provide new important insights into the regulation of activity-dependent gene expression.

In our laboratory, Sugo and his colleagues performed single-molecule imaging of a well-characterized transcription factor, CREB (Sugo et al., 2015). They demonstrated that neuronal activity increased frequent reappearance of fluorescent-tagged CREB spots at fixed nuclear locations in the time range of several seconds in mouse cortical neurons (Kitagawa et al., 2017). These results indicate that activity-dependent transcription can induce via frequent binding of CREB to specific gene loci. The next intriguing question is how CREB interacts with CBP and other transcription-related proteins in an activity-dependent manner.

Another crucial problem of understanding the molecular mechanism of activity-dependent gene expression is that only a few studies have performed using human neurons. A large number of previous studies that have elucidated

these mechanisms using model animals including rodents. There are two reasons why I elucidate the mechanism of activity-dependent gene expression in human neurons: the relevance of diseases and evolution. First, it has been reported that the linking neuropsychiatric disorders to abnormalities of the expression of activity-dependent genes (Ebert and Greenberg, 2013; Boulting et al., 2021). CBP and its paralog P300 are known to be causal genes of Rubinstein-Taybi syndrome, which causes mental retardation and intellectual disability (Petrij et al., 1995). Moreover, some other genes that regulate the expression of activity-dependent genes are also reported as causal genes for neuropsychiatric diseases (Amir et al., 1999; Hanauer and Young, 2002; Splawski et al., 2004). Second, activity-dependent gene responsiveness differs depending on human and mouse neurons, and the species-dependent difference may result from evolutionary changes of mutations in transcriptional regulatory elements of activity-dependent genes (Qiu et al., 2016; Pruunsild et al., 2023). Therefore, it is important to investigate the mechanisms of activity-dependent gene expression in not only rodent but human neurons.

In the present thesis, I investigated how neuronal activity alters the interactions between CREB-DNA and CREB-CBP in human cortical neurons. In the first half of the thesis, I established a method of differentiation from human ES cells into cortical neurons, and examined how neuronal activity changed CREB dynamics at the single-molecule level using the culture. In the second half of the thesis, I analyzed whether single-molecule CREB dynamics is affected by CBP HAT activity and binding to CBP.

General introduction references

Adams DL, Sincich LC, Horton JC (2007) Complete pattern of ocular dominance columns in human primary visual cortex. J Neurosci 27:10391-10403.

Amir RE, Van den Veyver IB, Wan M, Tran CQ, Francke U, Zoghbi HY (1999) Rett syndrome is caused by mutations in X-linked MECP2, encoding methyl-CpG-binding protein 2. Nat Genet 23:185-188.

Andrews W, Liapi A, Plachez C, Camurri L, Zhang J, Mori S, Murakami F, Parnavelas JG, Sundaresan V, Richards LJ (2006) Robo1 regulates the development of major axon tracts and interneuron migration in the forebrain. Development 133:2243-2252.

Antonini A, Stryker MP (1993) Rapid remodeling of axonal arbors in the visual cortex. Science 260:1819-1821.

Antonini A, Stryker MP (1996) Plasticity of geniculocortical afferents following brief or prolonged monocular occlusion in the cat. J Comp Neurol 369:64-82.

Bagri A, Marín O, Plump AS, Mak J, Pleasure SJ, Rubenstein JL, Tessier-Lavigne M (2002) Slit proteins prevent midline crossing and determine the dorsoventral position of major axonal pathways in the mammalian forebrain. Neuron 33:233-248.

Bannister AJ, Kouzarides T (1996) The CBP co-activator is a histone acetyltransferase. Nature 384:641-643.

Boulting GL, Durresi E, Ataman B, Sherman MA, Mei K, Harmin DA, Carter AC, Hochbaum DR, Granger AJ, Engreitz JM, Hrvatin S, Blanchard MR, Yang MG, Griffith EC, Greenberg ME (2021) Activity-dependent regulome of human GABAergic neurons reveals new patterns of gene regulation and neurological disease heritability. Nat Neurosci 24:437-448.

Butts DA, Feller MB, Shatz CJ, Rokhsar DS (1999) Retinal waves are governed by collective network properties. J Neurosci 19:3580-3593.

Chen J, Zhang Z, Li L, Chen BC, Revyakin A, Hajj B, Legant W, Dahan M, Lionnet T, Betzig E, Tjian R, Liu Z (2014) Single-molecule dynamics of enhanceosome assembly in embryonic stem cells. Cell 156:1274-1285.

de Jonge WJ, Patel HP, Meeussen JVW, Lenstra TL (2022) Following the tracks: How transcription factor binding dynamics control transcription. Biophys J 121:1583-1592.

Ebert DH, Greenberg ME (2013) Activity-dependent neuronal signalling and autism spectrum disorder. Nature 493:327-337.

Erzurumlu RS, Gaspar P (2012) Development and critical period plasticity of the barrel cortex. Eur J Neurosci 35:1540-1553.

Fazeli A, Dickinson SL, Hermiston ML, Tighe RV, Steen RG, Small CG, Stoeckli ET, Keino-Masu K, Masu M, Rayburn H, Simons J, Bronson RT, Gordon JI, Tessier-Lavigne M, Weinberg RA (1997) Phenotype of mice lacking functional Deleted in colorectal cancer (Dcc) gene. Nature 386:796-804.

Flavell SW, Greenberg ME (2008) Signaling mechanisms linking neuronal activity to gene expression and plasticity of the nervous system. Annu Rev Neurosci 31:563-590.

Flint AC, Dammerman RS, Kriegstein AR (1999) Endogenous activation of metabotropic glutamate receptors in neocortical development causes neuronal calcium oscillations. Proc Natl Acad Sci U S A 96:12144-12149.

Fowler T, Sen R, Roy AL (2011) Regulation of primary response genes. Mol Cell 44:348-360.

Granseth B, Fukushima Y, Sugo N, Lagnado L, Yamamoto N (2013) Regulation of thalamocortical axon branching by BDNF and synaptic vesicle cycling. Front Neural Circuits 7:202.

Greer PL, Greenberg ME (2008) From synapse to nucleus: calcium-dependent gene transcription in the control of synapse development and function. Neuron 59:846-860.

Hanauer A, Young ID (2002) Coffin-Lowry syndrome: clinical and molecular features. J Med Genet 39:705-713.

Harris RM, Woolsey TA (1981) Dendritic plasticity in mouse barrel cortex following postnatal vibrissa follicle damage. J Comp Neurol 196:357-376.

Hayano Y, Sasaki K, Ohmura N, Takemoto M, Maeda Y, Yamashita T, Hata Y, Kitada K, Yamamoto N (2014) Netrin-4 regulates thalamocortical axon branching in an activity-dependent fashion. Proc Natl Acad Sci U S A 111:15226-15231.

Hipp L, Beer J, Kuchler O, Reisser M, Sinske D, Michaelis J, Gebhardt JCM, Knoll B (2019) Single-molecule imaging of the transcription factor SRF reveals prolonged chromatin-binding kinetics upon cell stimulation. Proc Natl Acad Sci U S A 116:880-889.

Horch HW, Katz LC (2002) BDNF release from single cells elicits local dendritic growth in nearby neurons. Nat Neurosci 5:1177-1184.

Hu Z, Yue X, Shi G, Yue Y, Crockett DP, Blair-Flynn J, Reuhl K, Tessarollo L, Zhou R (2003) Corpus callosum deficiency in transgenic mice expressing a truncated ephrin-A receptor. J Neurosci 23:10963-10970.

Hubel DH, Wiesel TN (1962) Receptive fields, binocular interaction and functional architecture in the cat's visual cortex. J Physiol 160:106-154.

Hubel DH, Wiesel TN (1968) Receptive fields and functional architecture of monkey striate cortex. J Physiol 195:215-243.

Hubel DH, Wiesel TN (1970) The period of susceptibility to the physiological effects of unilateral eye closure in kittens. J Physiol 206:419-436.

Kim SK, Liu X, Park J, Um D, Kilaru G, Chiang CM, Kang M, Huber KM, Kang K, Kim TK (2021) Functional coordination of BET family proteins underlies altered transcription associated with memory impairment in fragile X syndrome. Sci Adv 7.

Kim TK, Hemberg M, Gray JM, Costa AM, Bear DM, Wu J, Harmin DA, Laptewicz M, Barbara-Haley K, Kuersten S, Markenscoff-Papadimitriou E, Kuhl D, Bito H, Worley PF, Kreiman G, Greenberg ME (2010) Widespread transcription at neuronal activity-regulated enhancers. Nature 465:182-187.

Kitagawa H, Sugo N, Morimatsu M, Arai Y, Yanagida T, Yamamoto N (2017) Activity-Dependent Dynamics of the Transcription Factor of cAMP-Response Element Binding Protein in Cortical Neurons Revealed by Single-Molecule Imaging. J Neurosci 37:1-10.

Latham A, Paul DH (1971) Spontaneous activity of cerebellar Purkinje cells and their responses to impulses in climbing fibres. J Physiol 213:135-156.

Lee PR, Fields RD (2021) Activity-Dependent Gene Expression in Neurons. Neuroscientist 27:355-366.

Liu Z, Tjian R (2018) Visualizing transcription factor dynamics in living cells. J Cell Biol 217:1181-1191.

Liu Z, Legant WR, Chen BC, Li L, Grimm JB, Lavis LD, Betzig E, Tjian R (2014) 3D imaging of Sox2 enhancer clusters in embryonic stem cells. Elife 3:e04236.

Lonze BE, Ginty DD (2002) Function and regulation of CREB family transcription factors in the nervous system. Neuron 35:605-623.

Malik AN, Vierbuchen T, Hemberg M, Rubin AA, Ling E, Couch CH, Stroud H, Spiegel I, Farh KK, Harmin DA, Greenberg ME (2014) Genome-wide identification and characterization of functional neuronal activity-dependent enhancers. Nat Neurosci 17:1330-1339.

Mancini DN, Singh SM, Archer TK, Rodenhiser DI (1999) Site-specific DNA methylation in the neurofibromatosis (NF1) promoter interferes with binding of CREB and SP1 transcription factors. Oncogene 18:4108-4119.

Mayr B, Montminy M (2001) Transcriptional regulation by the phosphorylation-

dependent factor CREB. Nat Rev Mol Cell Biol 2:599-609.

Mazza D, Abernathy A, Golob N, Morisaki T, McNally JG (2012) A benchmark for chromatin binding measurements in live cells. Nucleic Acids Res 40:e119.

McAllister AK, Katz LC, Lo DC (1996) Neurotrophin regulation of cortical dendritic growth requires activity. Neuron 17:1057-1064.

Mikuni T, Uesaka N, Okuno H, Hirai H, Deisseroth K, Bito H, Kano M (2013) Arc/Arg3.1 is a postsynaptic mediator of activity-dependent synapse elimination in the developing cerebellum. Neuron 78:1024-1035.

Mire E, Mezzera C, Leyva-Díaz E, Paternain AV, Squarzoni P, Bluy L, Castillo-Paterna M, López MJ, Peregrín S, Tessier-Lavigne M, Garel S, Galcerán J, Lerma J, López-Bendito G (2012) Spontaneous activity regulates Robo1 transcription to mediate a switch in thalamocortical axon growth. Nat Neurosci 15:1134-1143.

Morè L, Privitera L, Perrett P, Cooper DD, Bonnello MVG, Arthur JSC, Frenguelli BG (2022) CREB serine 133 is necessary for spatial cognitive flexibility and long-term potentiation. Neuropharmacology 219:109237.

Mueller F, Mazza D, Stasevich TJ, McNally JG (2010) FRAP and kinetic modeling in the analysis of nuclear protein dynamics: what do we really know? Curr Opin Cell Biol 22:403-411.

Nishikimi M, Oishi K, Nakajima K (2013) Axon guidance mechanisms for establishment of callosal connections. Neural Plast 2013:149060.

Okamoto K, Fujita H, Okada Y, Shinkai S, Onami S, Abe K, Fujimoto K, Sasaki K, Shioi G, Watanabe TM (2023) Single-molecule tracking of Nanog and Oct4 in living mouse embryonic stem cells uncovers a feedback mechanism of pluripotency maintenance. Embo j 42:e112305.

Park H, Poo MM (2013) Neurotrophin regulation of neural circuit development and function. Nat Rev Neurosci 14:7-23.

Petrij F, Giles RH, Dauwerse HG, Saris JJ, Hennekam RC, Masuno M, Tommerup N, van Ommen GJ, Goodman RH, Peters DJ, et al. (1995) Rubinstein-Taybi syndrome caused by mutations in the transcriptional co-activator CBP. Nature 376:348-351.

Pruunsild P, Bengtson CP, Loss I, Lohrer B, Bading H (2023) Expression of the primate-specific LINC00473 RNA in mouse neurons promotes excitability and CREB-regulated transcription. J Biol Chem 299:104671.

Qiu J et al. (2016) Evidence for evolutionary divergence of activity-dependent gene expression in developing neurons. Elife 5.

Serafini T, Colamarino SA, Leonardo ED, Wang H, Beddington R, Skarnes WC, Tessier-Lavigne M (1996) Netrin-1 is required for commissural axon guidance in the

developing vertebrate nervous system. Cell 87:1001-1014.

Shatz CJ, Stryker MP (1988) Prenatal tetrodotoxin infusion blocks segregation of retinogeniculate afferents. Science 242:87-89.

Specht CG, Izeddin I, Rodriguez PC, El Beheiry M, Rostaing P, Darzacq X, Dahan M, Triller A (2013) Quantitative nanoscopy of inhibitory synapses: counting gephyrin molecules and receptor binding sites. Neuron 79:308-321.

Speil J, Baumgart E, Siebrasse JP, Veith R, Vinkemeier U, Kubitscheck U (2011) Activated STAT1 transcription factors conduct distinct saltatory movements in the cell nucleus. Biophys J 101:2592-2600.

Splawski I, Timothy KW, Sharpe LM, Decher N, Kumar P, Bloise R, Napolitano C, Schwartz PJ, Joseph RM, Condouris K, Tager-Flusberg H, Priori SG, Sanguinetti MC, Keating MT (2004) Ca(V)1.2 calcium channel dysfunction causes a multisystem disorder including arrhythmia and autism. Cell 119:19-31.

Sugo N, Morimatsu M, Arai Y, Kousoku Y, Ohkuni A, Nomura T, Yanagida T, Yamamoto N (2015) Single-Molecule Imaging Reveals Dynamics of CREB Transcription Factor Bound to Its Target Sequence. Sci Rep 5:10662.

Suzuki A, Fukushima H, Mukawa T, Toyoda H, Wu LJ, Zhao MG, Xu H, Shang Y, Endoh K, Iwamoto T, Mamiya N, Okano E, Hasegawa S, Mercaldo V, Zhang Y, Maeda R, Ohta M, Josselyn SA, Zhuo M, Kida S (2011) Upregulation of CREB-mediated transcription enhances both short- and long-term memory. J Neurosci 31:8786-8802.

Torborg CL, Feller MB (2005) Spontaneous patterned retinal activity and the refinement of retinal projections. Prog Neurobiol 76:213-235.

Tyssowski KM, DeStefino NR, Cho JH, Dunn CJ, Poston RG, Carty CE, Jones RD, Chang SM, Romeo P, Wurzelmann MK, Ward JM, Andermann ML, Saha RN, Dudek SM, Gray JM (2018) Different Neuronal Activity Patterns Induce Different Gene Expression Programs. Neuron 98:530-546 e511.

Uesaka N, Hayano Y, Yamada A, Yamamoto N (2007) Interplay between laminar specificity and activity-dependent mechanisms of thalamocortical axon branching. J Neurosci 27:5215-5223.

Van der Loos H, Woolsey TA (1973) Somatosensory cortex: structural alterations following early injury to sense organs. Science 179:395-398.

Wiesel TN, Hubel DH (1963) SINGLE-CELL RESPONSES IN STRIATE CORTEX OF KITTENS DEPRIVED OF VISION IN ONE EYE. J Neurophysiol 26:1003-1017.

Wilkerson JR, Tsai NP, Maksimova MA, Wu H, Cabalo NP, Loerwald KW, Dictenberg JB, Gibson JR, Huber KM (2014) A role for dendritic mGluR5-mediated local

translation of Arc/Arg3.1 in MEF2-dependent synapse elimination. Cell Rep 7:1589-1600.

Woolsey TA, Van der Loos H (1970) The structural organization of layer IV in the somatosensory region (SI) of mouse cerebral cortex. The description of a cortical field composed of discrete cytoarchitectonic units. Brain Res 17:205-242.

Yamamoto N, López-Bendito G (2012) Shaping brain connections through spontaneous neural activity. Eur J Neurosci 35:1595-1604.

Zhang X, Odom DT, Koo SH, Conkright MD, Canettieri G, Best J, Chen H, Jenner R, Herbolsheimer E, Jacobsen E, Kadam S, Ecker JR, Emerson B, Hogenesch JB, Unterman T, Young RA, Montminy M (2005) Genome-wide analysis of cAMP-response element binding protein occupancy, phosphorylation, and target gene activation in human tissues. Proc Natl Acad Sci U S A 102:4459-4464.

Zhou Y, Wu H, Li S, Chen Q, Cheng XW, Zheng J, Takemori H, Xiong ZQ (2006) Requirement of TORC1 for late-phase long-term potentiation in the hippocampus. PLoS One 1:e16.

Introduction

In the developing brain, sensory-evoked and spontaneous firing activity plays a key role in neuronal circuit remodeling and plasticity by controlling the expression of numerous activity-regulated genes that underlie axon and dendritic growth and synapse formation (West and Greenberg, 2011; Yamamoto and López-Bendito, 2012; Thompson et al., 2017; Pumo et al., 2022). The impairment of these processes leads to neurodevelopmental and neuropsychiatric disorders, emphasizing their importance for normal acquisition of human cognitive functions (Amir et al., 1999; Ebert and Greenberg, 2013; Boulting et al., 2021).

To date, biochemical studies have demonstrated the fundamental molecular mechanisms of activity-dependent gene transcription. Neuronal activity induces calcium influx and activates a subset of transcription factors, thereby regulating the expression of several hundreds of genes positively and negatively with different time courses (Hardingham et al., 2001; Impey et al., 2002; Greer and Greenberg, 2008; Fowler et al., 2011; Joo et al., 2016; Tyssowski et al., 2018; Miyasaka and Yamamoto, 2021). In particular, cAMP response element binding protein (CREB) is a well-characterized transcription factor for activity-dependent gene expression. Membrane depolarization induces rapid phosphorylation of CREB and its binding to CRE sequences, and initiates transcription accompanied by RNA polymerase II (RNAPII) recruitment (Bito et al., 1996; Mayr and Montminy, 2001; Kornhauser et al., 2002; Lonze and Ginty, 2002). An intriguing question is how neuronal activity affects CREB dynamics and induces

downstream gene expression spatiotemporally in the nucleus. Indeed, only a subset of CRE sites are transcriptionally activated in an activity-dependent manner (Zhang et al., 2005), suggesting that CREB binding to selective CRE sites depends on specific regulators.

The epigenetic regulation of chromatin accessibility could modify CREB-dependent transcription (Kim et al., 2010; Malik et al., 2014). CREB-binding protein (CBP) has been shown to contribute to the histone modification via acetyltransferase (HAT) activity that relaxes chromatin structures, followed by recruitment of RNAPII (Chrivia et al., 1993; Bannister and Kouzarides, 1996; Chen et al., 2019; Esvald et al., 2020). However, the role of CBP in CREB-dependent transcription is not fully uncovered. More specifically, how acetylated regions by CBP are distributed in the nucleus and how CBP interacts with CREB in response to neuronal activity remain unknown.

Here, I attempted to elucidate the spatiotemporal CREB and CBP dynamics in the nucleus which regulates the expression of activity-dependent genes, using single-molecule imaging (SMI) (Speil et al., 2011; Chen et al., 2014; Liu et al., 2014; Sugo et al., 2015; Kitagawa et al., 2017; Hipp et al., 2019), visualization of activated RNA polymerase (Ohishi et al., 2022; Uchino et al., 2022), live imaging of fluorescent-tagged molecules and mutant overexpression. In particular, SMI is efficient to exhibit spatiotemporal dynamic aspects of transcription factors and chromatin modifiers (Specht et al., 2013; Zhan et al., 2014; Nozaki et al., 2017; Renner et al., 2017; Kaplan et al., 2018; Yamamoto and Okada, 2020). Moreover, since CBP is a causative gene of

Rubinstein-Taybi syndrome whose patients show mental retardation and intellectual disability (Petrij et al., 1995; Spena et al., 2015; Korzus, 2017), I performed these experiments with human ES cell (ESC)-derived cortical neurons (Shi et al., 2012; Espuny-Camacho et al., 2013), in order to link my findings to potential pathophysiological mechanisms. These results demonstrated that neuronal activity induces frequent CREB-DNA and CREB-CBP interactions for several seconds in the nucleus, and that the repetitive CREB binding activated the transcription at predetermined histone acetylation sites.

Materials and Methods

Human ESC differentiation into cortical cells

All experiments using human ESCs and neural stem cells were conducted with the approval of the VIB, KU Leuven and Osaka University Ethical Committees. To generate human cortical cells, H9 ESCs were plated with human ES medium containing 10 μM ROCK-inhibitor Y27632 (Espuny-Camacho et al., 2013). Two days later (0 DIV), the medium was exchanged to the culture medium containing 100 ng/ml Noggin for 25 days. The obtained neural stem cells were further expanded for about a week and frozen in vials in liquid nitrogen. These frozen cells were used as neuroepithelial and radial glial cells for cortical cell differentiation. One day before plating, glass bottomed dishes (Greiner Bio-One, 627860) were coated by 0.1 mg/ml Poly-L-ornithine (Sigma, P3655) for longer than 3 h and subsequently by Matrigel (Corning, 356234) only in the center of dishes (5 mm diameter) for at least 2 h. After thawing, 1-2 x 10^4 cells were plated at the Matrigel-coated area with the culture medium. The medium was replaced every one week. The culture medium consisted of a 1:1 mixture of DDM/B27 and Nb/B27. DDM/B27 consisted of DMEM/F-12 (gibco, 11320-033) supplemented with 1% GlutaMAX (gibco,355050-061), 1% N2, 2% B27 (minus vitamin A), 0.05% BSA Fraction solution (gibco, 15260-037), 100 nM β-ME, 1% MEM NEAA (gibco, 11140-050), 1% Penicillin Streptomycin (gibco, 15070-063) and 1 mM Sodium Pyruvate (gibco, 11360-070). Nb/B27 consisted of Neurobasal Medium (gibco, 21103-049) supplemented with 2% B27, 1% Penicillin Streptomycin and 1% L-Glutamine (nacalai, 16919-42). These

cultures were maintained at 37 °C in an environment of humidified 95% air and 5% CO2.

Plasmids

To study CREB dynamics at the single-molecule level, a Tet-inducible HaloTag-CREB expression vector, pTet-On Advance/TRE-Tight HaloTag-human CREB, was used (Kitagawa et al., 2017). To label neurons, α tubulin promoter-driven EGFP (pTα1-EGFP) or Dsred2 (pTα1-Dsred) expression vectors was used (Hatanaka and Murakami, 2002). To perform optogenetic stimulation, pCAGGS-hChR2(H134R)-EYFP was used. To visualize accumulation of RNAPII, pB533-44B12mut23-sfGFP encoding GFP-tagged Ser5ph RNAPII-specific probe was used (Ohishi et al., 2022). Commercially available pCMV-GFP-BRD4 (addgene, 65378) was used to examine BRD4 distribution in live imaging (Gong et al., 2015). To generate pCAGGS-EGFP-CBP expression vector, human CBP cDNA (Promega, pFN24K) was inserted into AsisI and PmeI sites in pCAGGS-EGFP. To make a CBP mutation in HAT domain (Y1540A/F1541A) (Korzus et al., 2004), pCAGGS-EGFP-CBP was amplified by PCR with the mutagenesis primer pairs: 5'-TGGGCCAGAAATCACCTTCAGCAGCGGGCAGTTCCTTGGCACTGG-3' and 5'- CCAGTGCCAAGGAACTGCCCGCTGCTGAAGGTGATTTCTGGCCCA -3'. The PCR product and pCAGGS-EGFP-CBP were digested by AsisI and PmeI, and human CBP mutant (dHAT) was inserted. To generate pTRE-SNAPtag-CBP, pTRE-tight SNAPtag-TORC1 was digested by AsisI and PmeI sites, and

human CBP cDNA was inserted. To generate pTRE-SNAPtag alone, human CBP was digested by AsisI and PmeI sites. To generate pTet-On Advance/TRE-Tight HaloTag-human CREB (Y134F), a CREB mutation was performed. The PCR product and pTet-On Advance/TRE-Tight HaloTag-human CREB was digested by AsisI and PmeI, and human CREB mutant (Y134F) was inserted. All plasmids were harvested using Maxiprep Kit (Qiagen, 12163 or 12362).

Pharmacological experiment

To stimulate cultured cells, 0.41 volumes of KCl depolarization solution (170 mM KCl, 1.3 mM MgCl2, 0.9 mM CaCl2, 10 mM HEPES, pH 7.4) was added to the culture medium 1 h before the SMI (Kitagawa et al., 2017). To examine the expression levels of FOS, BRD4 and H4ac using immunocytochemistry, the depolarization solution was added 3 h before fixation.

***In vitro* electroporation**

Transfection of the plasmids into cultured neurons was performed with an electroporation technique (Kitagawa et al., 2017). In brief, 0.1-0.5 μg/μl plasmid solution in 0.2 mL PBS was added to cultured cells on the glass bottomed dishes, and electric pulses composed of one 275 V pulse of 7 ms duration and five 20 V pulses of 50 ms duration were applied at 50 ms intervals through plate electrodes (CUY21EX, BEX). The cultures were washed with PBS and immersed in the original culture medium.

SMI

For the expression of HaloTag-CREB, cells were electroporated with pTet-On Advance/TRE-Tight HaloTag-human CREB (wild type, R301L or Y134F) (Sugo et al., 2015; Kitagawa et al., 2017; Yamamoto and Okada, 2020). One day before observation, 10-50 ng/ml doxycycline (Clontech, 631311) was added to the medium. To visualize HaloTag-CREB, the cultures were incubated with DMEM/F-12 containing 10 nM TMR direct-conjugated HaloTag ligand (Promega, G2991) or SaraFluor 650T-conjugated HaloTag ligand (Goryo Chemical, A308-01) for 15-30 min at 37°C.

An inverted microscope (Ti-E, Nikon) with an oil-immersion objective lens (x100, numerical aperture 1.49, Nikon) and HILO illumination was used to perform single-molecular imaging. The final magnification was 107 nm/pixel. The glass bottomed dish was mounted on a stage top incubator (Tokai Hit) and maintained at 37°C in a humidified atmosphere (5% CO2/95% air). Either TMR or 650T was visualized by HILO illumination with 561 nm (20 mW, Coherent) or 640 nm (40 mW, Coherent) lasers, respectively. Images were obtained at 10 frames per second for 2 min using an EM-CCD (iXon897, Andor Technology) with Solis software (Andor Technology).

To perform simultaneous imaging of HaloTag-CREB and SNAPtag-CBP or SNAPtag alone, cells were electroporated with pTet-On Advance/TRE-Tight HaloTag-CREB and pTRE-SNAPtag-CBP or pTRE-SNAPtag alone. After adding doxycycline, the transfected cells were incubated with a mixture of TMR-conjugated HaloTag ligand and 647SiR-conjugated SNAPtag ligand (NEB,

S9102S). Both fluorescent dyes were excited by HILO illumination with 561 nm and 640 nm lasers. The images obtained by simultaneous excitation were separated using an image splitting optics W-VIEW GEMINI (Hamamatsu Photonics) with a 640 nm long-pass dichroic mirror (Semrock FF640-FDi01-25x36), and were collected using two bypass filters (Semrock FF01-593/40-25 for 593 nm and FF01-692/40-25 for 692 nm). Split images were obtained at 10 frames per second for 1-2 min using the EM-CCD with NIS-Elements software (Nikon). Aberration had been corrected using 0.1 μm TetraSpeck Fluorescent Microspheres (ThermoFisher, T7284).

For simultaneous observation of HaloTag-CREB at the single-molecule level and Ser5ph RNAPII-GFP signals, cells were electroporated with pTet-On Advance/TRE-Tight HaloTag-CREB and pB533-44B12mut23-sfGFP. After adding doxycycline, the transfected cells were incubated with 650T HaloTag ligand, and HILO illumination with 640 nm and 488 nm (20 mW, Coherent) lasers was used for excitation. The obtained images were separated using the image splitting optics and collected via two bypass filters (Edmund Optics 86951 for 525 nm and Semrock FF01-692/40-25 for 692 nm), as described above.

To examine the spatial relationship between BRD4 and CREB, pCMV-GFP-BRD4 was cotransfected with pTet-On Advance/TRE-Tight HaloTag-CREB. Before and after SMI of CREB, GFP signal containing images were collected under epi-fluorescent excitation light (488 nm, Nikon).

Immunocytochemistry

Cultured cells were fixed with 4% paraformaldehyde in PBS at room temperature for 10 min or 1 h. For staining for VGLUT1 and PSD95, the cells were fixed with 1% paraformaldehyde at room temperature for 3 min, followed by ice-cold methanol for 15 min. After incubation with PBS containing 0.3% Triton X-100 (PBST) for 30 min, the cells were subjected to primary antibodies in a blocking buffer, composed of 2% normal donkey serum (Jackson ImmunoResearch, 017-000-121) or normal goat serum (Vector laboratory, S-1000) in PBST at 4°C for overnight. After washing, the cells were incubated with secondary antibodies in PBST at room temperature for 2 h. After washing, the cells were mounted by a medium containing 80% glycerol and 2.3% 1,4-diazabicyclo [2.2.2] octane (Sigma-Aldrich, D2522-25G), and 0.1% 4',6-diamidino-2-phenylimdole (DAPI, Sigma-Aldrich) in 50 mM Tris-HCl. Finally, the cells were observed with a Axioskop 2 plus (Zeiss) or confocal microscopy, DM6000 CS (Leica). Primary antibodies were anti-TBR1 (rabbit polyclonal, Abcam, ab31940), anti-CTIP2 (rat monoclonal, Abcam, ab18465), anti-MAP2 (mouse monoclonal, Sigma, M1406), anti-BRN2 (goat polyclonal, Santa Cruz, sc-6029), anti-GFAP (rabbit polyclonal, Sigma, G9269), anti-VGLUT1 (rabbit polyclonal, Synaptic Systems, 135303), anti-PSD95 (mouse monoclonal, Abcam, ab2723), anti-CREB (mouse monoclonal, Cell Signaling Technology, 9104), anti-Phosphorylated CREB (Ser133) (rabbit monoclonal, Cell Signaling Technology, 9198), anti-FOS (rabbit polyclonal, Abcam, ab190289), anti-BRD4 (rabbit monoclonal, Abcam, ab128874) and anti-acetyl-Histone H4 (rabbit

polyclonal, Sigma, 06-866). Secondary antibodies were anti-rabbit IgG Alexa Flour 488 (goat polyclonal, Thermo Fisher, A11034), anti-goat IgG Alexa Flour 488 (donkey polyclonal, Abcam, ab150129), anti-rat IgG Cy3 (Goat Polyclonal, Millipore, AP183C), anti-mouse IgG Cy3 (donkey polyclonal, Millipore, AP192C), anti-mouse IgG Alexa Flour 594 (donkey polyclonal, Thermo Fisher, A21203) and anti-mouse IgG Cy5 (goat polyclonal, Jackson ImmunoResearch, 115-175-166).

Interactions between CREB and CRE in cell-free conditions using SMI

A flow cell assembled from two cover glasses was prepared (Sugo et al., 2015). Biotin-labeled dsDNAs (40 nM in PBS) were adsorbed onto the cover glass surface. Biotin-labeled 19-nt dsDNA including the CRE sequence was prepared by annealing 5'-GACAGCGCACGTCAAGGCA-biotin -3' and its complementary oligonucleotide. Biotin-labeled 22-nt dsDNA including the κB sequence was prepared by annealing 5'-AGTTGAGGGGACTTTCCCAGGC-biotin-3' and its complementary oligonucleotide. The flow cell was treated with 10 mg/ml BSA in PBS for 5 min and then flushed with a binding buffer solution (100 mM KCl, 1 mM MgCl2, 20 mM HEPES-NaOH (pH 7.8), 0.1 M DTT, 2 mg/ml BSA, 50% sucrose). In experiments, TMR-CREB in binding buffer was loaded into the flow cell. HaloTag CREB proteins were generated by the TNT Quick Coupled Transcription/Translation System (Promega) with plasmids encoding HaloTag-human CREB1 cDNA (Promega) and labeled with HaloTag TMR Ligand (Promega).

Optogenetic stimulation

An optogenetic experiment was performed by applying excitation light to ChR2-transfected cells (Malyshevskaya et al., 2013; Kitagawa et al., 2017; Miyasaka and Yamamoto, 2021). In brief, a solid-state illuminator (475 nm, 20 mW, Lumencor SPECTRA) was used under the control of a stimulator (A.M.P.I, Master-9). The light stimulation (50 ms duration) was applied with 2 Hz for 5 min through a 100x objective lens.

RNA fluorescence *in situ* hybridization coupled with immunocytochemistry

RNA FISH experiments combined with immunocytochemistry were carried out according to manufacturer's instruction (https://biosearchassets.blob.core.windows.net/assets/bti_custom_stellaris_immunofluorescence_protocol.pdf, LGC Biosearch) with a slight modification. Stellaris RNA FISH Probes were customized for human *FOS* intron with Quasar 570, human *NR4A1* intron with Quasar 670 and human *GAPDH* intron with Quasar 670 (LGC Biosearch). Cells on the glass bottom dishes were fixed in 3.7% formaldehyde (SIGMA, F8775-25ML) at room temperature for 10 min, and permeabilized in 70% ethanol at 4°C for overnight. The cells were hybridized with 125 nM of the RNA probes in hybridization buffer at 37°C for 4-16 h, and incubated with first antibodies at 4°C for overnight and with secondary antibodies in PBST at room temperature for 2 h. The cells were mounted with Antifade Mounting Medium (Vector Laboratories, H-1000) containing 5 ng/ml

DAPI. Fifty z-stacks with a 0.2 μm step size and 100 ms exposure time were obtained using the EM-CCD, and deconvolved by NIS-Elements software (Nikon).

Spatiotemporal analysis of SMI

All fluorescence images were analyzed by ImageJ software with a plugin, Particle Track and Analysis (Sugo et al., 2015; Kitagawa et al., 2017) and Origin software (OriginLab). To quantify the temporal dynamics of individual CREB spots, the center coordinate of each spot was determined (using x/y) by Gaussian fitting, and the residence time was measured. The cumulative residence time distribution was fitted by the sum of two exponential curves, $F(t) = A_0 + A_1 (1 - \exp(- t/t_1)) + A_2 (1 - \exp(- t/t_2))$ (Equation 1), using the Levenberg-Marquardt chi-square minimization algorithm. A_0 is constant. A_1 and A_2 are the fractions with time constants t_1 and t_2, respectively ($t_1 < t_2$). When the chi-square tolerance value was less than 1×10^{-9}, the fit was deemed appropriate. Similarly, single-molecule CBP spots were tracked and the residence time distribution was fitted by Equation 1.

To determine the time which separates the long and short residence components, the time was calculated such that the ratio of the short residence component, $A_1 \exp(- t/t_1) / (A_0 + A_1 \exp(- t/t_1) + A_2 \exp(- t/t_2))$, is sufficiently small (< 3%). As a result, the boundary times for CREB and CBP spots were determined to be 1 s and 0.6 s, respectively.

To quantify the spatial features of CREB dynamics, the micro-domain was determined by the sum of the maximum fluctuation of the estimated center coordinates for long residence CREB spots and the microscopic stage movement over a 2-min live imaging period. The fluctuation ranges (1.96□ for the center coordinates) were determined by fitting the motion of CREB spots into a Gaussian distribution. The maximum value of fluctuation for TMR- or 650T-CREB (3.7 pixel, 0.40 μm, n = 44 spots) was then added to the microscopic stage movement (1.0 ± 0.1 pixel, 0.11 ± 0.01 μm, n = 20 spots), and the sum was defined as one-side of the micro-domain (0.54 x 0.54 μm, 5 x 5 pixel).

To quantify repetitive CREB appearance, the area covering the whole nucleus in a neuron was divided into 1024 (32 x 32) equal micro-domains. The number of long residence CREB spots was counted in each micro-domain, and normalized by the total number of long residence CREB spots. This value was used as frequency. Mean and SD of the frequency were calculated for all micro-domains under the unstimulated condition. The micro-domains with > mean + 4 SD, which were hardly observed in the unstimulated condition, were defined as a hotspot.

Analysis of RNAPII distribution with single-molecule CREB

As described above, RNAPII-GFP images were obtained simultaneously with SMI of HaloTag-CREB. RNAPII-GFP images were averaged per 32 frames as the signals were rather noisy. $(F-F_0)/F_0$ was referred as the relative intensity of

Ser5ph RNAPII-GFP. F is the GFP intensity, and F_0 is the average of F from 0 s to 10 s. To quantify the correlation between CREB spots and RNAPII-GFP signals, the number of long residence CREB spots and the time integral values of RNAPII-GFP for the CREB residence time plus the subsequent 10 s were calculated for each micro-domain. In this analysis, the subnuclear domain for RNAPII-GFP was defined as 10 pixels square (1.07 x 1.07 μm) because the signals were broader than those for CREB spots (see Figure 8A).

Quantification of BRD4 and H4ac signals after immunocytochemistry

Immunostaining images with anti-BRD4 and anti-H4ac were obtained by 50 z-stacks with a 0.2 μm step size. After the background subtraction, the number and the volume of these spots per cell were measured by ImageJ.

Colocalization analyses

As for colocalization of CREB and CBP during simultaneous live imaging, when the distance between the center coordinates of TMR-CREB and 647SiR-CBP is smaller than the sum of fluctuation ranges of CREB (0.10 ± 0.01 μm, n = 22 spots) and those of CBP (0.10 ± 0.01 μm, n = 26 spots), these spots were defined as colocalization (0.20 μm = 0.10 + 0.10). The fluctuation was obtained by fitting the motion into a 2D Gaussian distribution, and a value twice the standard deviation was used as the fluctuation range.

As for colocalization of 650T-CREB and GFP-BRD4 spots, when the distance between the center coordinates of 650T-CREB and GFP-BRD4 spots was

smaller than the sum of the fluctuation ranges of CREB spots (0.13 ± 0.01 μm, n = 44 spots), the radius of GFP-BRD4 spots (0.29 ± 0.01 μm, n = 36 spots, the radius was used since GFP-BRD4 spots were not single molecules) and the microscopic stage movement over a 2-min live imaging period (0.11 ± 0.01 μm, n = 20 spots), these spots were defined as colocalization (0.53 μm = 0.13 + 0.29 + 0.11). The spatial distribution of GFP-BRD4 spot intensities was fitted by a 2D Gaussian distribution, and a value twice the standard deviation was used as the radius.

As for colocalization of RNA FISH with immunopositive spots, when the distance between the center coordinates of two spots was smaller than the sum of the radii of these two spots, these two spots were defined as colocalization. The radius of each spot was determined similarly to BRD4-GFP as these spots also did not represent single molecules. The radii were 0.27 ± 0.01 μm for *FOS* (n = 32 alleles), 0.32 ± 0.01 μm for *NR4A1* (n = 27 alleles), 0.26 ± 0.01 μm for immunopositive BRD4 (n = 47 spots) and 0.26 ± 0.00 μm for immunopositive H4ac (n = 59 spots). As a result, the sum of radii was 0.53 μm (0.27 + 0.26 μm) for *FOS* and BRD4, 0.58 μm (0.32 + 0.26 μm) for *NR4A1* and BRD4, and 0.53 μm (0.27 + 0.26 μm) for *FOS* and H4ac.

Time delay of appearance and disappearance of long residence CREB spots colocalized with CBP spots (> 0.6 s) was calculated from the residence time of each spot, although the order of dissociation between these spots may be unclear as it is possible that colocalized signals are quenching.

Statistical analysis

Statistical analyses were done by Origin 2021 or R software (x64 version 3.5.1) software. In comparison between the two distribution, Kolmogorov-Smirnov test was performed. A comparison between the two groups was performed with the Mann-Whitney U test. For comparison among more than three groups, Kruskal-Wallis ANOVA with Dunn's post hoc test or one-way ANOVA with Tukey-Kramer post hoc test was used. For pairwise comparisons, Chi-square test was performed. For comparison against theoretical mean, one-sample t test was done. In all statistics, $p < 0.05$ was considered significant. Bar graphs and scatter plots show mean values and error bars show SEM. In, all box-and-whiskers plots, boxes indicate 25-75% quantiles and the median line, whiskers indicate 10-90% quantiles and squares indicate the mean.

Results

Human ESC-derived cortical neurons respond to neuronal activity

To study activity-dependent CREB dynamics in human cortical neurons, I established an *in vitro* system in which human cortical pyramidal neurons are generated from ESCs and cultured in monolayer so that SMI can be performed (Espuny-Camacho et al., 2013). For anterior neural induction, H9 ESCs were first differentiated into neuroepithelial and radial glia cells for 25 days *in vitro* (DIV), followed by differentiation into cortical neurons (Figure 1A). Immunocytochemistry showed that many cells expressed MAP2 and the deep layer neuron markers (TBR1 and CTIP2) about 60 DIV after neural induction (Figure 1B). Up to 90 DIV after neural induction, a small number of cells expressed the upper layer neuron marker BRN2 and the astrocyte marker GFAP (Figure 1C and 1D). The presynaptic marker VGLUT1 and the postsynaptic marker PSD95 were also expressed at this later stage (Figure 1E). These data showed that human ESCs differentiated into cortical neurons according to the order of cortical development, which is consistent with the previous results (Shi et al., 2012; Espuny-Camacho et al., 2013; Linaro et al., 2019).

To confirm whether neuronal activity induces activity-dependent gene expression in this culture, the expression of activated CREB and its target genes, FOS and NR4A1 was examined in the depolarized condition by increasing extracellular KCl (Bading et al., 1993). Immunocytochemistry showed

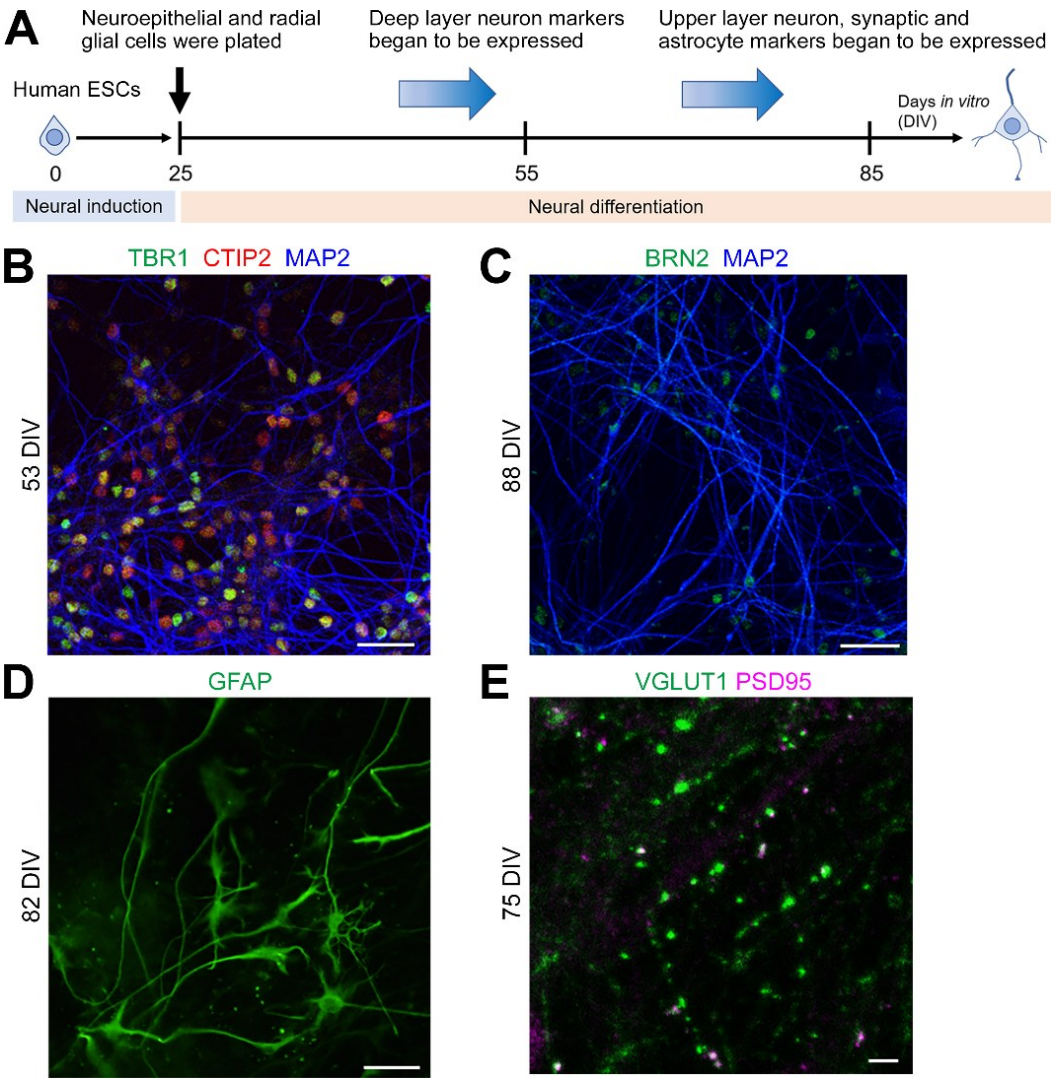

Figure 1. Human ESCs differentiation into cortical neurons.

(A) The scheme of differentiation from human ESCs into cortical cells. Human ESCs differentiate into neuroepithelial and radial glial cells, and they subsequently differentiate into cortical cells (deep layer neurons, upper layer neurons and glial cells). (B-D) Immunocytochemistry showed the identity of cells differentiated from human ESCs. Many cells expressed deep layer neuron markers (TBR1 and CTIP2) within 2 months. A few neurons expressed an upper layer neuron marker (BRN2) and astrocyte marker (GFAP) in 2-3 months. In (B-D), scale bars, 50 μm. (E) Pre (VGLUT1) and post (PSD95) synaptic markers were also expressed in 2-3 months. Scale bar, 5 μm.

that KCl treatment induced expression of Ser133 phosphorylated CREB and FOS in cultured neurons while CREB expression was observed regardless of KCl treatment (Figure 2A and B). Although the intensities of phosphorylated CREB varied among cells, most cells (86.5 %, n = 104 cells) exhibited immunopositive signals in KCl treatment. In addition, RNA FISH with intron probes and immunocytochemistry with anti-CREB showed that the transcripts of *FOS* and *NR4A1*, but not *GAPDH*, were present at CREB-positive locations in the nucleus of KCl-treated neurons (Figure 2C-E). Thus, typical activity-dependent events such as CREB activation and the downstream gene expression occurred in human ESC-derived cortical neurons.

SMI demonstrates CREB binding to DNA

To investigate single-molecule CREB dynamics, a Tet-inducible HaloTag-CREB expression vector was transfected with a neuron-specific promoter-driven reporter (pTα1-EGFP) by electroporation in cultured cells at approximately 60 DIV, and was visualized by Tetramethylrhodamine (TMR) or 650T-conjugated HaloTag ligand (Figure 3A) (Sugo et al., 2015; Kitagawa et al., 2017). Highly inclined and laminated optical sheet (HILO) illumination (Figure 3B) showed that numerous fluorescent-labeled CREB spots appeared and disappeared in the nucleus of pTα1-EGFP-positive neurons (Figure 3C, Movie 1) (Tokunaga et al., 2008). When CREB spots were subjected to photobleaching under fixation condition, one-stepwise or two-stepwise reduction of fluorescence intensity was found (Figure 4A and B), indicating that observed CREB spots are detected at

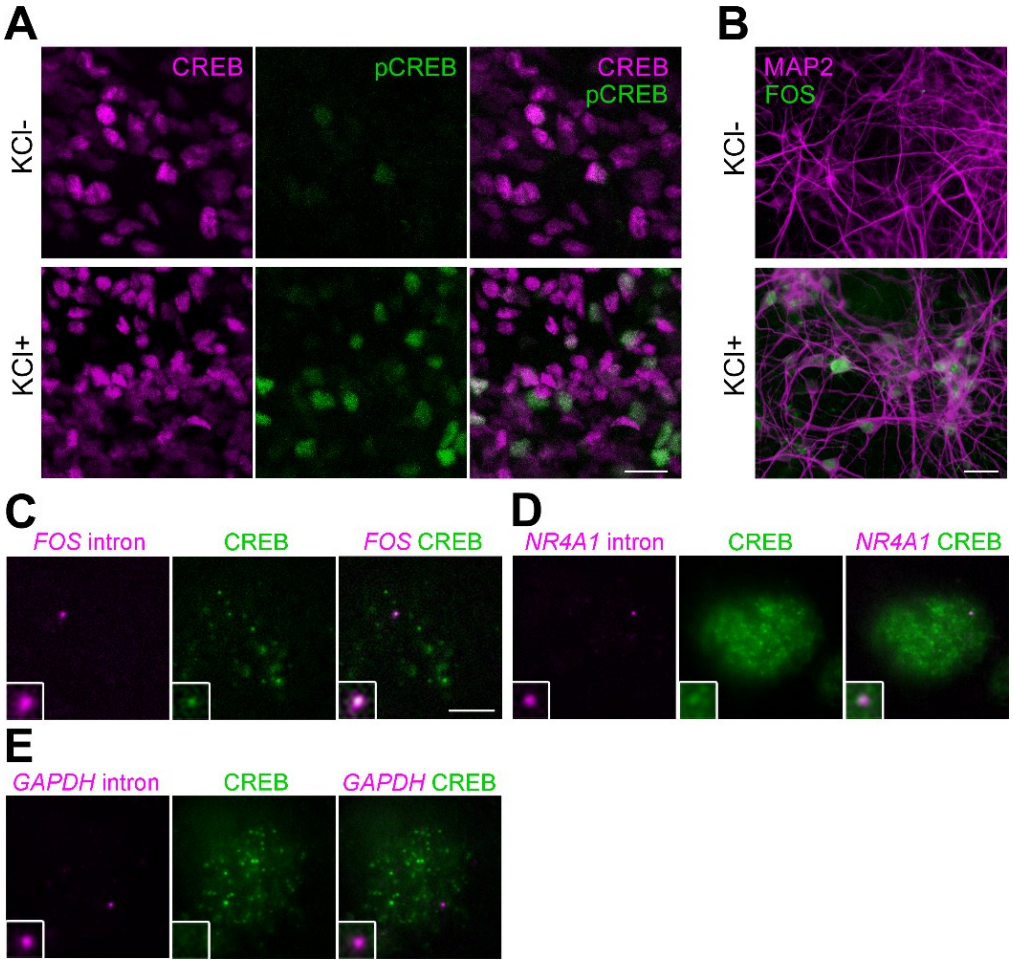

Figure 2. Activity-dependent gene expression via CREB in human ESC-derived cortical neurons.

(A) Immunocytochemistry for CREB and Ser133 phosphorylated CREB (pCREB) in human ESC-derived cortical neurons at 45 DIV with and without KCl treatment for 30 min. (B) Immunocytochemistry for FOS in human ESC-derived neurons at 53 DIV with and without KCl treatment. Most cells (86.5 %) expressed FOS signals in KCl treatment (n = 104 cells). In (A and B), scale bars, 20 μm. (C-E) Immunocytochemistry for CREB together with RNA FISH using FOS (C), NR4A1 (D) and GAPDH (E) intron probes was performed. Active transcription sites of FOS and NR4A1 colocalized with CREB foci while that of GAPDH hardly colocalized. Higher magnification images were indicated in lower left panels. Scale bar, 5 μm.

the single-molecule level, as CREB forms homodimer (Mayr and Montminy, 2001; Kitagawa et al., 2017). Moreover, the expression level of HaloTag-CREB was confirmed to be very low compared with the endogenous level (Figure 4C-F).

To characterize the CREB dynamics, I measured the residence time of each CREB spot over a 2-min observation period, and the residence time distribution was determined (Figure 3D). While most CREB spots (> 90%) disappeared quickly, a small but a significant number of CREB spots resided at the same locations on the order of seconds. I assumed that CREB spots with the long residence time might represent specific binding to CRE sites. Indeed, long residence components were markedly reduced, when CREB dynamics was examined using mutant CREB (R301L) which lacks DNA binding (Figure 3D) (Walton et al., 1992). Quantitative analysis further showed that the residence time distribution could be fitted by the sum of two exponential curves with distinct time constants (short and long residence component; Equation 1 in Materials and Methods) and that the ratio of the long to short residence component (A_2/A_1) was considerably smaller in CREB (R301L) than in wild-type CREB (0.18 ± 0.02 for wild type, 0.05 ± 0.01 for R301L, $p < 0.001$, Mann-Whitney U test) (Figure 3E, Table 1). This result suggests that CREB spots displaying long residence time represent specific binding to CRE, while CREB spots with short residence time represent non-specific binding to DNA or free moving. Hereafter CREB spots with residence times longer than 1 s were referred to as “long residence CREB spots”. Indeed, the exponential component

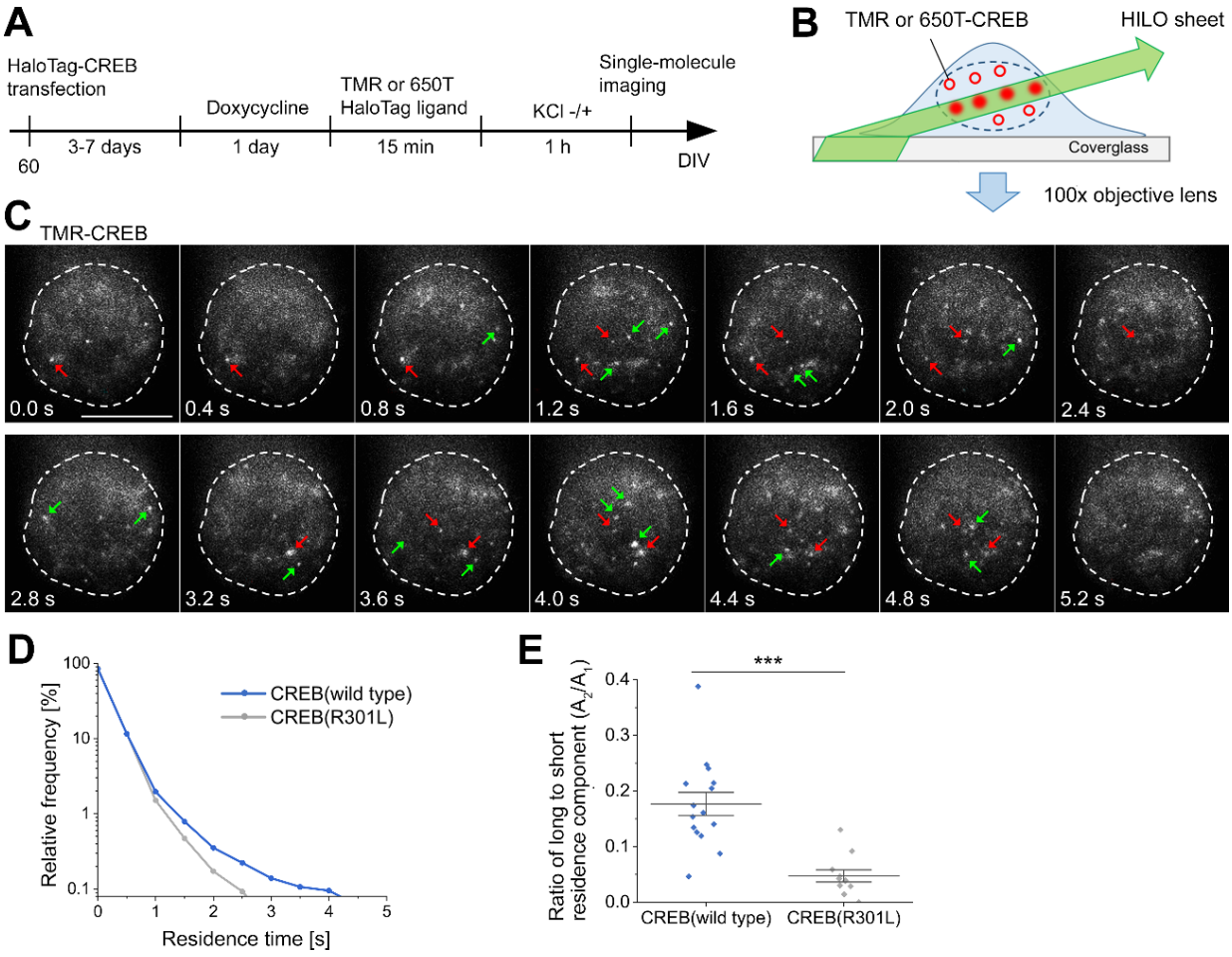

Figure 3. SMI of CREB dynamics in human ESC-derived cortical neurons. (A) Experimental timeline of CREB SMI in human ESC-derived neurons. (B) Schematic drawing of HILO microscopy for SMI. TMR or 650T-CREB was excited by HILO illumination, and fluorescence images were obtained at the single-molecule level. (C) Representative timelapse images of TMR-CREB in the Tα1-EGFP positive neuron without KCl treatment. Red arrows indicate TMR-CREB spots which stayed at the same location for longer than 1 sec. Green arrows indicate TMR-CREB spots which stayed for less than 1 sec. Dashed lines indicate the outline of the nucleus. Scale bar, 10 μm. (D) The residence time distribution of CREB (wild type) and CREB (R301L). The residence time was significantly shorter in mutant CREB (R301L) than wild-type CREB (***$p = 6.4 \times 10^{-10}$, Kolmogorov-Smirnov test). (E) The ratio of long to short residence component (A_2/A_1) was markedly smaller in CREB (R301L)

than in wild-type CREB (***p < 0.001, Mann-Whitney U test). Mean ± SEM. In (D and E), n = 15 cells for CREB (wild type), n = 11 cells for CREB (R301L).

	# of cells	# of cultures	t_1 [s]	t_2 [s]	A_2/A_1
CREB (wild type)	15	7	0.28 ± 0.02	2.20 ± 0.25	0.18 ± 0.02
CREB (R301L)	11	3	0.23 ± 0.01	1.19 ± 0.17**	0.05 ± 0.01***

Table 1. Dissociation rate constants and ratios of long- to short-residence components of wild-type and mutant CREB spots.

Asterisks indicate that the ratio of long-residence to short-residence component of mutant CREB (R301L) was significantly different from that of wild-type CREB (**p<0.01, ***p<0.001, Mann–Whitney U test). The values represent mean ± SEM.

with the short time constant had little contribution to the residence time distribution longer than 1 s (see Materials and Methods). Furthermore, SMI of CREB in cell-free conditions demonstrated that the same HaloTag-CREB single molecules resided for a long period on CRE sequence-containing DNA-coated substratum but not on κB sequence (Figure 5) (Sugo et al., 2015; Kitagawa et al., 2017), indicating that HaloTag-CREB functions in cultured cells while retaining its sequence-specific binding property.

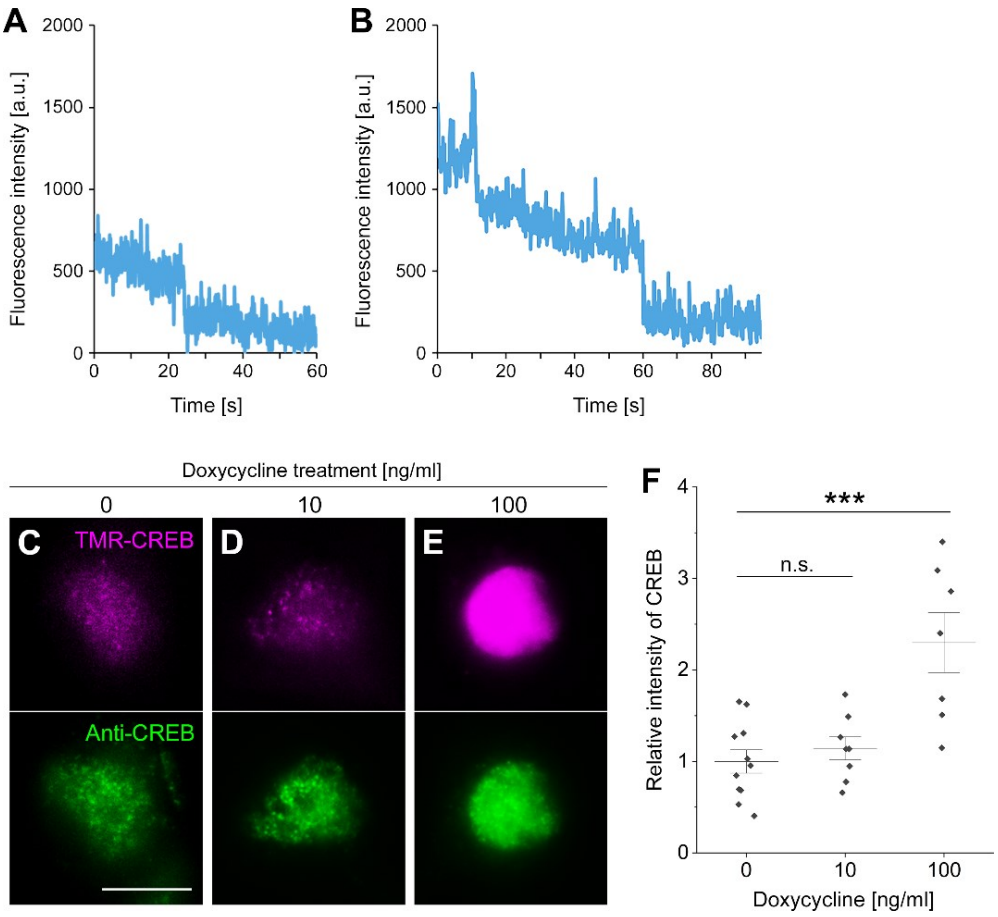

Figure 4. Single-molecule CREB expression level.

(A and B) HaloTag-CREB spots exhibited one-stepwise (A) or two-stepwise (B) reduction of the fluorescence intensities by photobleaching after fixation. (C-E) Representative images of HaloTag-CREB and immunocytochemistry with CREB antibody when adding different concentration of doxycycline (0, 10, 100 ng/ml). (F) The expression level of anti-CREB, which recognizes both endogenous and HaloTag-CREB, was very similar between 0 and 10 ng/ml doxycycline-treated cells whereas it was much increased in 100 ng/ml doxycycline-treated cells (***$p<0.001$, one-way ANOVA with Tukey-Kramer post hoc test, n = 11 cells in 0 ng/ml, n = 8 cells in 10 ng/ml, n = 7 cells in 100 ng/ml doxycycline treatment). Scale bar, 5 μm.

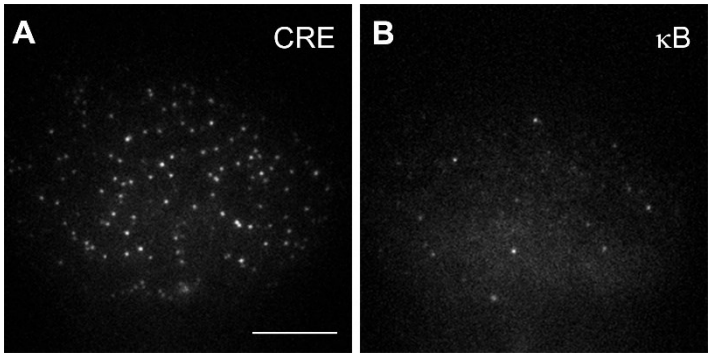

Figure 5. Single-molecule CREB binding to CRE sequence in cell-free conditions.

Representative images of HaloTag-CREB in cell-free conditions. HaloTag-CREB resided for a long period on CRE sequence-containing DNA-coated substratum (A) but not on κB sequence DNA-coated substratum (B). Scale bar, 10 μm.

Neuronal activity increases repetitive appearance of CREB, leading to phosphorylated RNAPII accumulation

Next, I investigated how neuronal activity alters the CREB dynamics. Under 1 h KCl treatment, the residence time distribution of CREB was found to be similar to that without KCl treatment (Figure 6A). A_2/A_1 was also unchanged by KCl treatment (0.18 ± 0.02 for KCl-, 0.17 ± 0.01 for KCl+, p = 0.78, Mann-Whitney U test) (Figure 6B, Table 2). Thus, it is unlikely that neuronal activity affects kinetics of individual CREB molecules. However, I found that CREB spots with long residence time appeared repetitively at the same nuclear locations (Figure 6C). In fact, the number of long residence CREB spots emerging at micro-domains (0.54 x 0.54 μm, see Materials and Methods) was increased by KCl treatment (Figure 6D). When the micro-domains with the highly repetitive

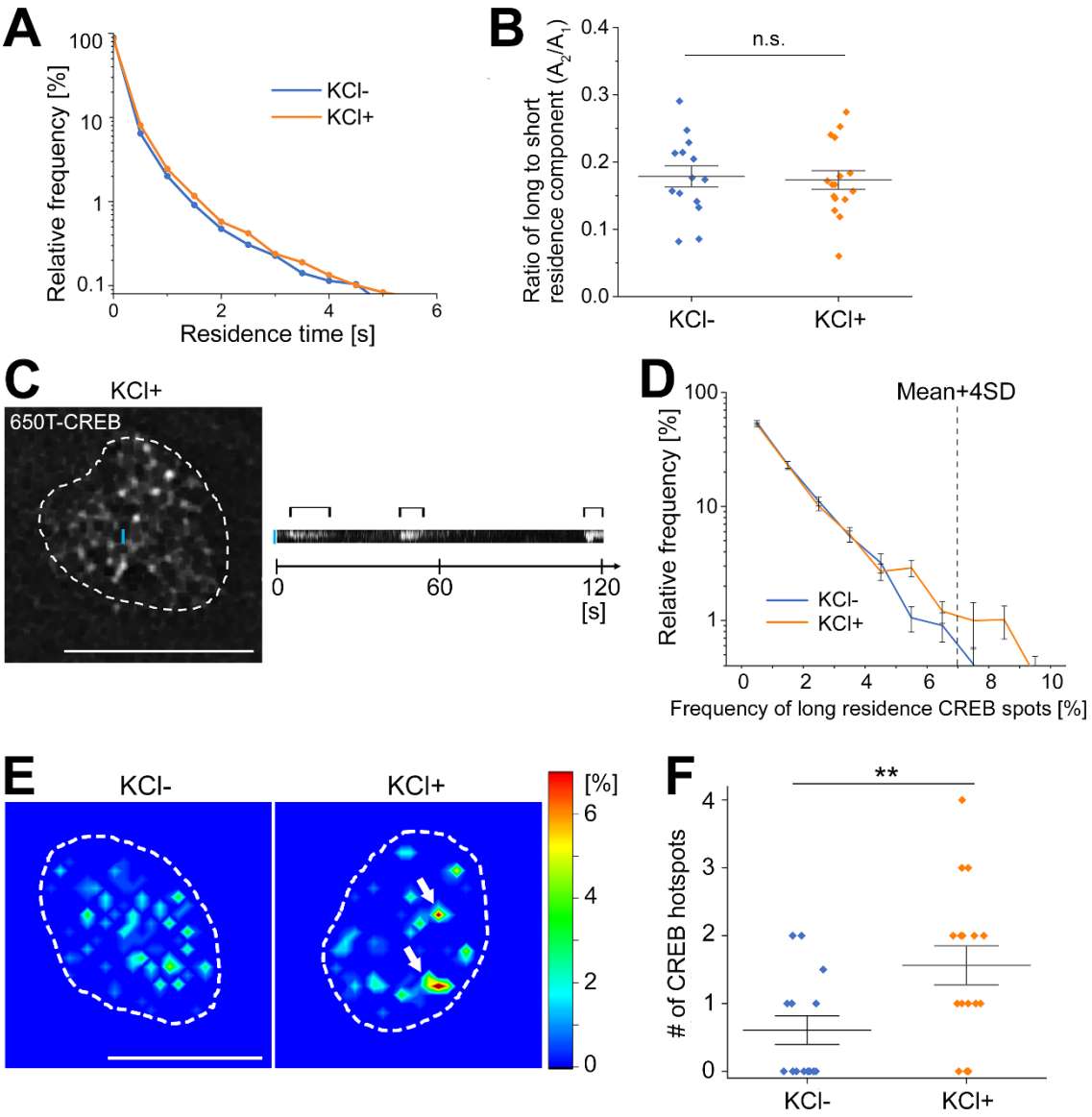

Figure 6. The increase of repetitive CREB emergence at fixed nuclear locations by neuronal stimulation.

(A and B) The residence time distribution and A_2/A_1 of CREB were very similar between KCl-untreated and -treated neurons. p = 0.42, Kolmogorov-Smirnov test in (A). p = 0.70, Mann-Whitney U test in (B). (C) Left, a representative 650T-CREB image in a KCl-treated neuron. Right, the kymograph shows that long residence CREB spots appeared repeatedly (black brackets) at a restricted location (blue line) of the nucleus during 2 min. The blue line length is 0.8 μm. (D and E) The area covering the whole nucleus in a neuron was divided into 1024 (32 x 32) equal micro-domains (0.54 x 0.54 μm). The number of long residence CREB spots over a 2-min observation period was counted in each

micro-domain, and divided by the total number of long residence CREB spots. This value was determined as frequency. The frequency was increased by KCl treatment (D). Color contour maps represent the spatial distribution of the frequency. Two CREB hotspots (> Mean +4SD, indicated by white arrows) were observed in the KCl-treated neuron while there was no hotspot in the KCl-untreated neuron. (F) The number of hotspots was significantly increased by KCl treatment (**p < 0.01, Mann-Whitney U test). In (A, B, D and F), n = 14 cells in KCl-untreated neurons, n = 16 cells for KCl-treated neurons. In (C, E), dashed lines represent the perimeter of the nuclei, and scale bars, 10 μm.

	# of cells	# of cultures	t_1 [s]	t_2 [s]	A_2/A_1	# of hotspots
KCl-	14	6	0.31 ± 0.01	2.15 ± 0.16	0.18 ± 0.02	0.6 ± 0.2
KCl+	16	6	0.30 ± 0.01	2.03 ± 0.22	0.17 ± 0.01	1.6 ± 0.3**

Table 2. Dissociation rate constants, ratios of the long- to short-residence component and the numbers of hotspots of CREB spots in response to KCl depolarization.

Asterisks indicate that the number of hotspots in KCl+ neurons was significantly different from that in KCl- neurons (**p<0.01, Mann–Whitney U test). The values represent mean ± SEM.

appearance of long residence CREB spots were defined as hotspots (> mean + 4 SD, see Materials and Methods), the number of hotspots was significantly higher in KCl-treated neurons than in untreated neurons (0.6 ± 0.2 for KCl-, 1.6 ± 0.3 for KCl+, p < 0.01, Mann-Whitney U test) (Figure 6E, F, Table 2).

This activity-dependent aspect was also examined in ChR2-expressing cells by applying optogenetic stimulation. Similar to the result of KCl treatment,

photostimulation (2 Hz, 5 min) increased the number of hotspots (0.6 ± 0.3 before photostimulation, 1.7 ± 0.3 after photostimulation, $p < 0.05$, Mann-Whitney U test), while the residence time distribution and A_2/A_1 were not changed (Figure 7, Table 3). Consistent with the previous study in mouse cortical neurons (Kitagawa et al., 2017), these results suggest that neuronal activity enhances repetitive CREB-CRE interaction at particular nuclear locations.

Such repetitive emergence of CREB spots may lead to the downstream gene expression. To test this possibility, I investigated the spatial relationship between long residence CREB spots and RNAPII accumulation (Cook, 1999; Yao et al., 2007; Li et al., 2019). Since phosphorylated RNAPII works during transcription (Buratowski, 2009), a plasmid encoding GFP-tagged Ser5ph RNAPII-specific probe (Ohishi et al., 2022; Uchino et al., 2022) was co-transfected with the HaloTag-CREB expression vector, and then simultaneous live imaging of the RNAPII distribution and single-molecule CREB was performed. RNAPII-GFP signals tended to be overlapped with the locations where long residence CREB spots appeared repetitively (white arrows in Figure 8A), although the GFP signals were spread out and broader than those for CREB spots. Moreover, the GFP intensities were increased temporally at the locations where long residence CREB spots appeared repeatedly, while it was almost unchanged at the sites where long residence CREB spots scarcely appeared (Figure 8B). The quantitative analysis showed that the time integral values of the localized GFP signals were well correlated with the number of long residence CREB spots

(Pearson's rank correlation coefficient, 0.87, $p = 5.5 \times 10^{-13}$) (see Materials and Methods, Figure 8C), suggesting that RNAPII is recruited at nuclear locations where long residence CREB spots repeatedly appear to induce activity-dependent gene expression.

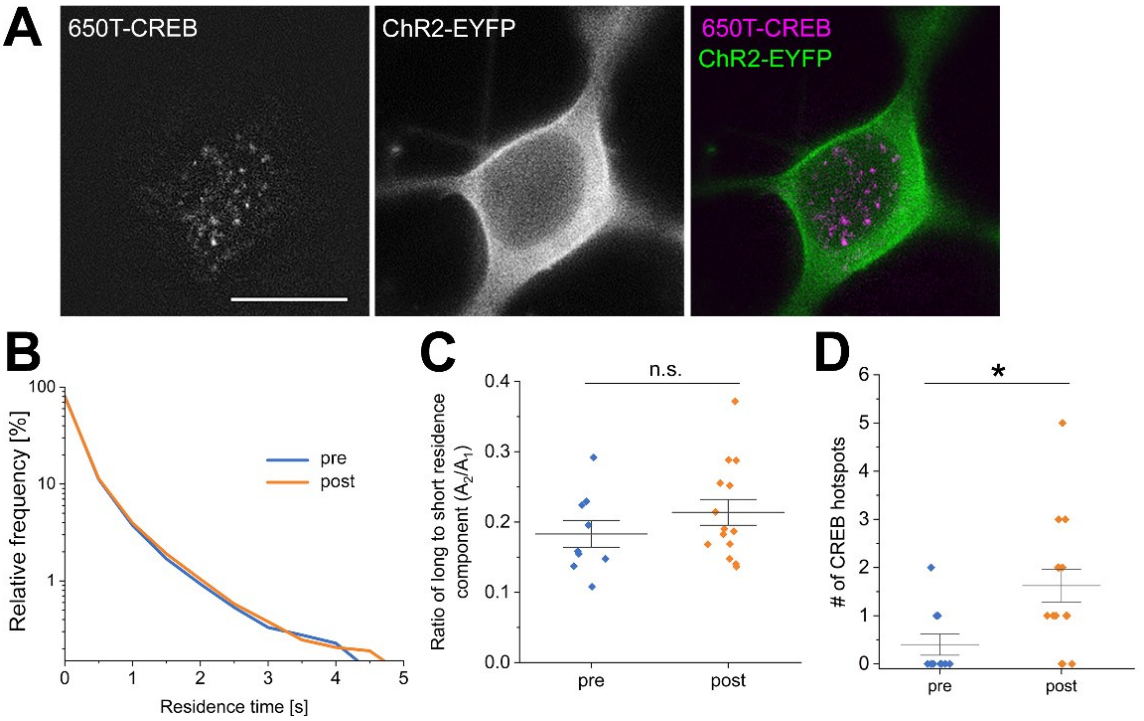

Figure 7. Single-molecule CREB dynamics under optogenetic stimulation. (A) A HaloTag-CREB expression vector was co-transfected with ChR2-EYFP in cultured cortical cells, and visualized by 650T-conjugated HaloTag ligand. Scale bar, 10 μm. (B and C) Photostimulation (2 Hz, 5 min) did not affect the residence time distribution ($p = 0.59$, Kolmogorov-Smirnov test) and A2/A1 ($p = 0.36$, Mann-Whitney U test). (D) The number of hotspots was significantly increased by photostimulation (*$p < 0.05$, Mann-Whitney U test). n = 9 cells.

	# of cells	# of cultures	t1 [s]	t2 [s]	A2/A1	# of hotspots
Before	9	3	0.35 ± 0.01	1.89 ± 0.11	0.18 ± 0.02	0.6 ± 0.3
After	9	3	0.36 ± 0.01	2.07 ± 0.17	0.21 ± 0.02	1.7 ± 0.3*

Table 3. Dissociation rate constants, ratios of the long- to short-residence component and the numbers of hotspots of CREB spots by optogenetic stimulation.

Asterisks indicate that the number of hotspots after photostimulation was significantly different from that before photostimulation (*p<0.05, Mann–Whitney U test). The values represent mean ± SEM.

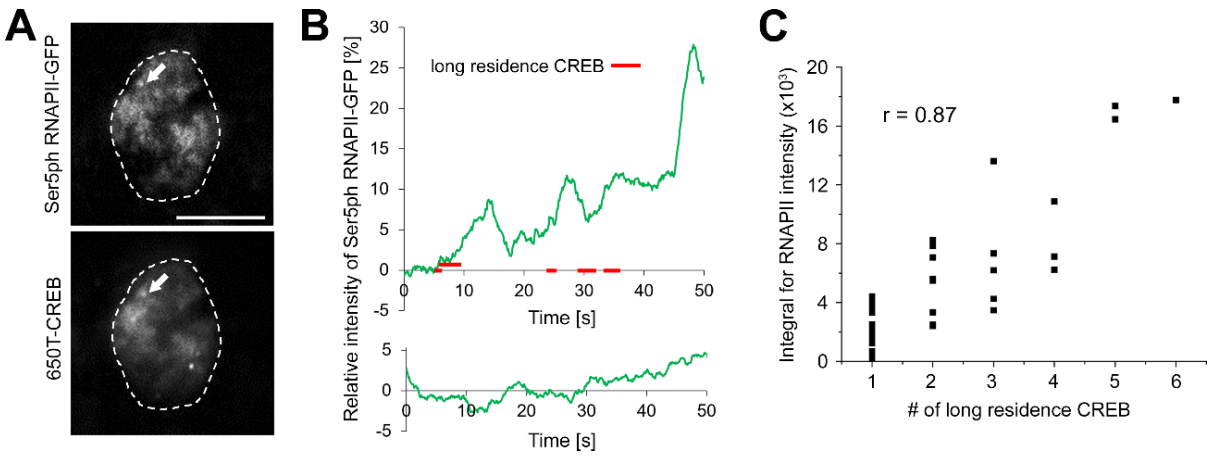

Figure 8. RNAPII accumulation at repetitive CREB-CRE binding sites.

(A) Representative images of 650T-CREB and Ser5ph RNAPII-GFP. A 650T-CREB spot colocalized with Ser5ph RNAPII-GFP signals (indicated by white arrows). Dashed lines represent the perimeter of the nuclei. Scale bars, 10 μm. (B) Representative time courses of Ser5ph RNAPII-GFP intensity and CREB spots appearance at one micro-domain (1.07 x 1.07 μm). Green lines show relative fluorescence intensity of Ser5ph RNAPII-GFP. Red bars show appearance of long residence CREB spots. Long residence CREB spots appeared repeatedly in the upper panel while any long residence CREB spot was not observed in the lower panel. (C) The number of long residence CREB spots per micro-domain was strongly correlated with the time integral values of

Ser5ph RNAPII-GFP intensity. Pearson's correlation coefficient: r is 0.87 ($p = 5.5 \times 10^{-13}$ for 40 micro-domains with long residence CREB spots).

Activity-dependent repetitive CREB binding promotes transcription at histone acetylation sites

Since histone acetylation contributes to activity-dependent transcription (Malik et al., 2014; Chen et al., 2019), I hypothesized that repetitive CREB-DNA interaction and the subsequent transcription could take place at acetylated chromatin regions. As bromodomain containing proteins are known to recognize histone acetylation (Marmorstein and Zhou, 2014), GFP-tagged bromodomain containing 4 (BRD4) was used to mark acetylated regions in live imaging of CREB (Filippakopoulos et al., 2012; Loven et al., 2013).

The spatial relationship between CREB hotspots and BRD4 signals was examined in GFP-BRD4 expressing human cortical cells. For this, a GFP-BRD4 expression plasmid was co-transfected with the HaloTag-CREB plasmid. In the nucleus of cortical neurons, GFP-BRD4 was widely distributed with dotted-like structures. Under KCl treatment, the locations of CREB hotspots were determined by SMI as described above, and were compared to GFP-BRD4 spots. As shown in Figure 9A, CREB hotspots tended to appear at GFP-BRD4 spots. The quantitative analysis showed that roughly two-thirds of CREB hotspots colocalized with GFP-BRD4 spots, while randomly distributed nuclear locations exhibited little colocalization ($p < 0.001$, Chi-square test, see Materials and Methods) (Figure 9B and 9C).

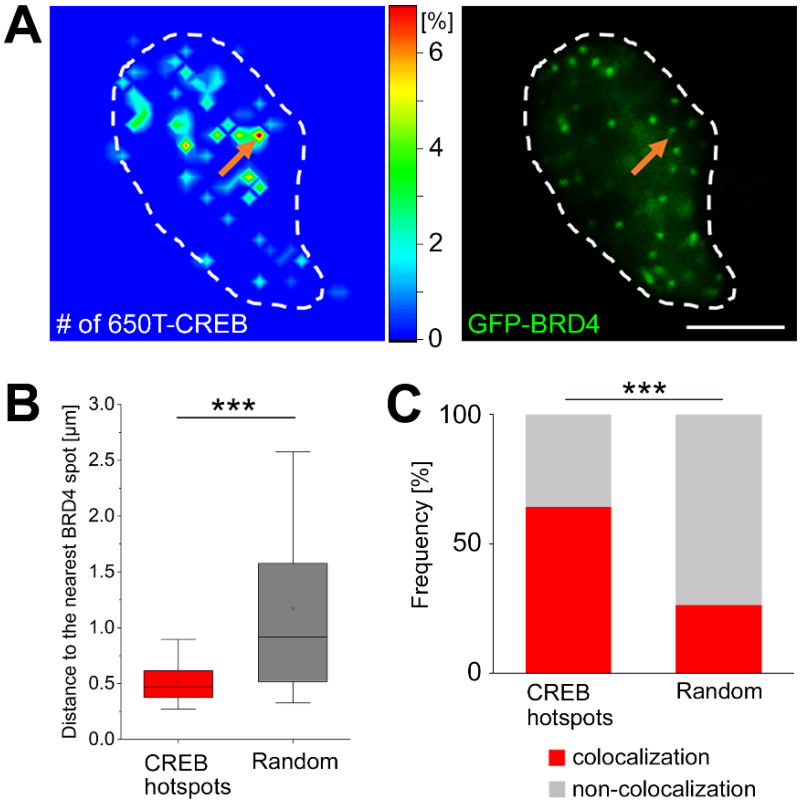

Figure 9. Activity-dependent repetitive CREB-CRE binding at BRD4-positive sites.

(A) Similar to Figure 6E, the number of CREB spots over a 2-min observation period was counted in each micro-domain (0.54 x 0.54 μm). Color contour map showing the spatial distribution of the frequency of long residence CREB appearance having long residence times (left) and GFP-BRD4 (right) in KCl-treated cell. A CREB hotspot colocalized with a BRD4 spot (indicated by orange arrows). Dashed lines represent the perimeter of the nuclei. Scale bars, 5 μm. (B) Distances from CREB hotspots to the nearest GFP-BRD4 spots were significantly smaller than those from randomized nuclear positions to the nearest GFP-BRD4 spots (***$p < 0.001$, Mann-Whitney U test). (C) The colocalization frequency of CREB hotspots with BRD4 signals was higher than when hotspots were randomly distributed in the nucleus (***$p < 0.001$, Chi-square test). In (B and C), n=259 spots of 10 cells.

As repetitive CREB binding to DNA would promote downstream gene transcription, the spatial relation was also examined between endogenous BRD4 spots and transcription sites of activity-dependent genes. For this, RNA FISH analysis using intron probes of *FOS* and *NR4A1* was carried out together with immunocytochemistry for BRD4 (Zhang et al., 2005; Tyssowski et al., 2018). As shown in Figure 10A and C, one or two *FOS* and *NR4A1* active transcription sites were detected in KCl-treated neurons, whereas they were hardly detected in KCl-untreated neurons (Figure 10G and H). In KCl-treated cultures, these *FOS* spots were often colocalized with BRD4 spots. The analysis of colocalization demonstrated that more than two-thirds of *FOS* transcription sites colocalized with BRD4 spots, significantly higher than if transcription was assumed to occur randomly ($p < 0.001$, Chi-square test, see Materials and Methods) (Figure 10B and 10C). Similarly, the majority of *NR4A1* transcription sites were colocalized with BRD4 signals in KCl-treated neurons, and the ratio was also significantly higher than the randomized condition ($p < 0.01$, Chi-square test) (Figure 10E and 10F). These results imply that repetitive CREB binding to CRE promotes transcription of the early response genes at histone acetylation sites.

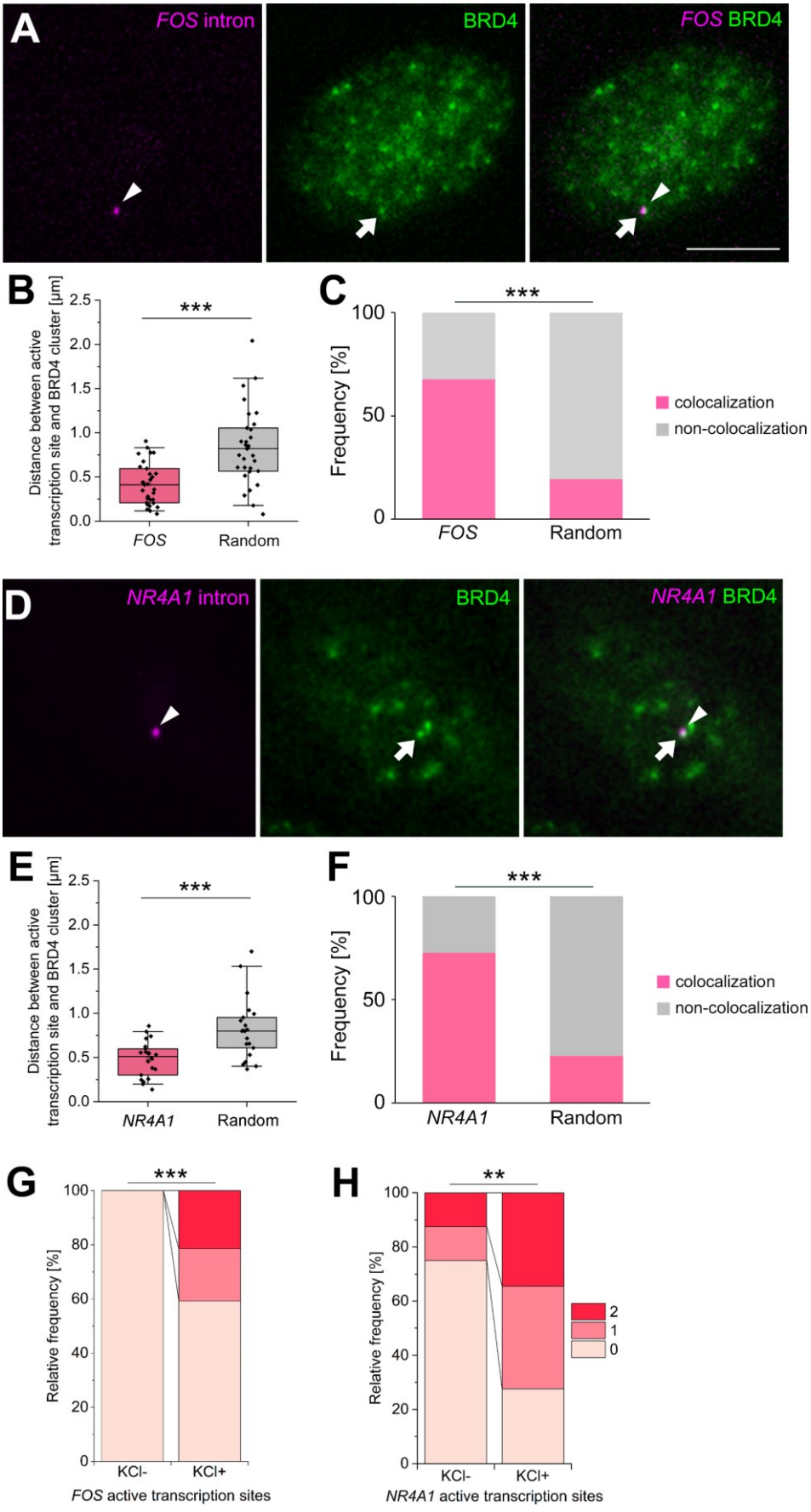
A
FOS intron
BRD4
FOS BRD4
B
***
Distance between active transcription site and BRD4 cluster [µm]
2.5
2.0
1.5
1.0
0.5
0.0
FOS
Random
C
***
Frequency [%]
100
50
0
FOS
Random
colocalization
non-colocalization
D
NR4A1 intron
BRD4
NR4A1 BRD4
E
***
Distance between active transcription site and BRD4 cluster [µm]
2.5
2.0
1.5
1.0
0.5
0.0
NR4A1
Random
F
***
Frequency [%]
100
50
0
NR4A1
Random
colocalization
non-colocalization
G
***
Relative frequency [%]
100
80
60
40
20
0
KCl-
KCl+
FOS active transcription sites
H
**
Relative frequency [%]
100
80
60
40
20
0
KCl-
KCl+
NR4A1 active transcription sites
2
1
0

Figure 10. Activity-dependent gene transcription at BRD4-positive sites. (A and C) Active transcription sites of *FOS* (A) and *NR4A1* (C) colocalized with BRD4 spots (indicated by arrows) in 30 min KCl treatment. Active transcription sites were indicated by arrowheads. Scale bars, 5 μm. (B and E) Distances from *FOS* and *NR4A1* spots to the nearest BRD4 spots were significantly smaller than those from randomized nuclear positions (***p < 0.001, Mann-Whitney U test). Based on the distance, the cases where distance between given two spots was less than the sum of average radii were defined as colocalization (see Materials and Methods). (C and F) The colocalization frequency of active transcription sites with BRD4 spots was significantly higher than the cases where the transcription sites were distributed randomly (***p < 0.001, Chi-square test. In (A-F), n=31 alleles for *FOS* and n=22 alleles for *NR4A1*. (G and H) The number of FOS and NR4A1 active transcription sites (either 0, 1 or 2) was strikingly increased by KCl treatment (**p < 0.01, ***p < 0.001, Chi-square test). FOS: n = 32 alleles in KCl-untreated cells, n = 98 alleles in KCl-treated cells. NR4A1: n = 16 alleles in KCl-untreated cells, n = 34 alleles in KCl-treated cells.

CBP HAT activity is essential for CREB-DNA binding

The next question is what activity produces these acetylated sites recognized by BRD4. As HAT activity of CBP may be involved in CREB-dependent transcription (Bannister and Kouzarides, 1996), the involvement was examined by inhibiting CBP HAT activity. After overexpression of EGFP-tagged mutant CBP lacking HAT activity (dHAT CBP) (Figure 11A) (Korzus et al., 2004), immunocytochemistry with anti-BRD4 showed that BRD4 signals were rather weak in dHAT CBP-expressing neurons (Figure 11B and C). Quantitative analysis showed that the number of BRD4 spots was significantly decreased by dHAT CBP expression (50.5 ± 2.8 for control, 29.3 ± 1.7 for dHAT CBP, p < 0.001, one-way ANOVA with Tukey Kramer test) (Figure 11D). The total volume

of BRD4 spots was also significantly smaller in dHAT CBP-expressing neurons (Figure 11E).

The effect of dHAT CBP on histone acetylation sites was also investigated by histone H4 acetylation (H4ac), as BRD4 may not localize in all of the acetylated sites. Immunocytochemistry with anti-H4ac (K5, 8, 12 and 16) showed that H4ac was also distributed in a dotted manner in the nucleus, and that *FOS* transcription sites largely colocalized with H4ac spots (Figure 12). Thus, H4ac sites are also likely involved in activity-dependent gene expression. In dHAT CBP-expressing cells the number of H4ac spots was significantly smaller than control cells (46.8 ± 2.4 for control, 30.3 ± 2.2 for dHAT CBP, $p < 0.001$, one-way ANOVA with Tukey Kramer test) (Figure 11F and G), which is similar to the effect on BRD4 spots. These results indicate that the formation of histone acetylation sites in the nucleus strongly depends on CBP HAT activity.

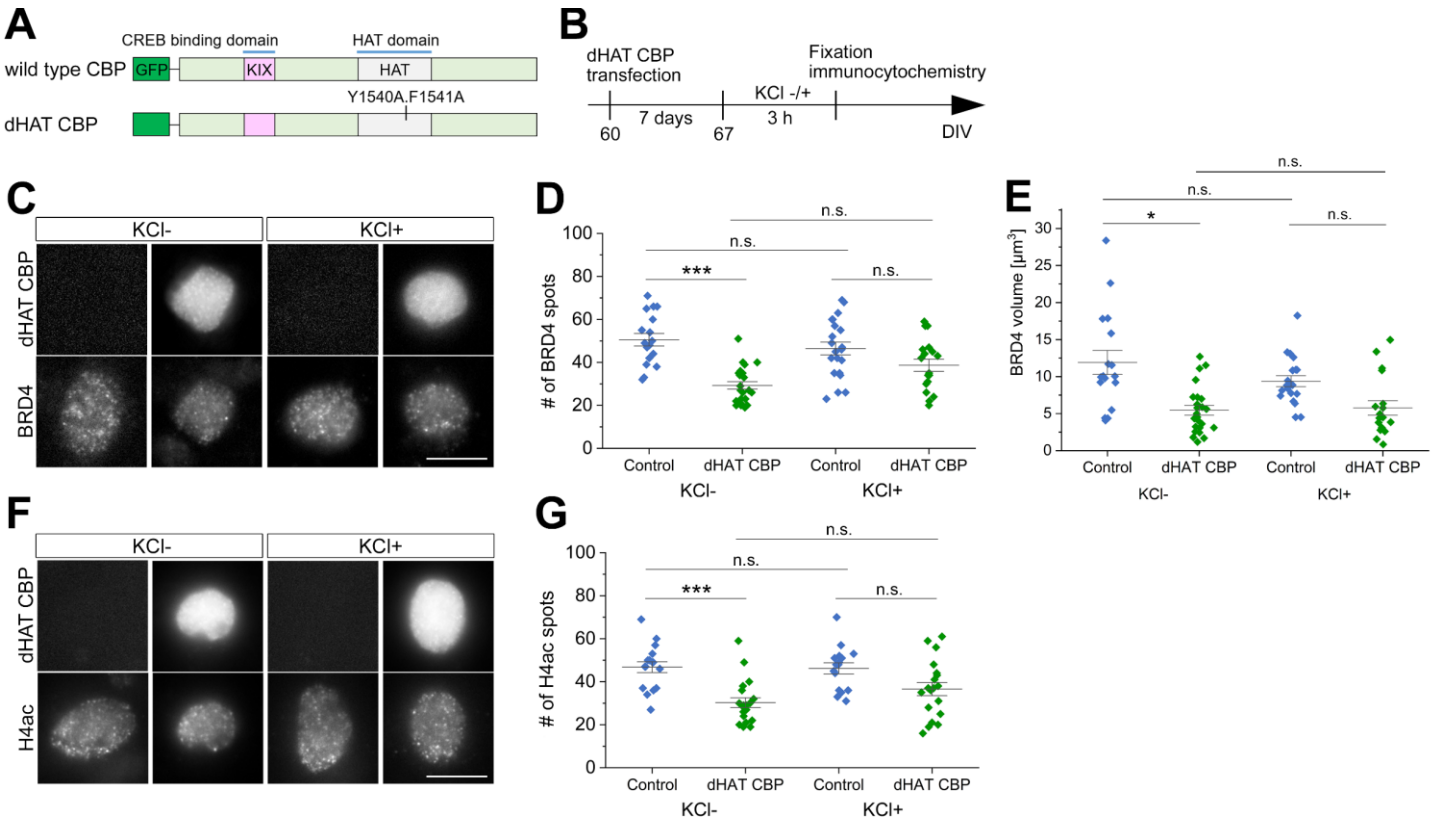

Figure 11. The formation of histone acetylation sites by CBP HAT activity. (A) Human CBP structure and the location of missense mutations (Y1540A.F1541A) in HAT domain. (B) Experimental timeline of dHAT CBP overexpression. (C) Representative images of BRD4 signals in dHAT CBP-positive neurons. (D) The number of BRD4 spots per cell in dHAT CBP-expressing neurons was significantly smaller than in control neurons (***p < 0.001, one-way ANOVA with Tukey-Kramer post hoc test). On the other hand, regardless of dHAT CBP expression, the number of BRD4 spots did not change under KCl stimulation (p > 0.05, one-way ANOVA with Tukey-Kramer post hoc test). n = 17 cells in control neurons, n = 24 cells in dHAT CBP-expressing neurons, n = 21 cells in KCl-treated neurons, n = 18 cells in dHAT CBP-expressing and KCl-treated neurons. (E) Total BRD4 volume per cell in dHAT CBP-expressing neurons was significantly smaller than in control neurons (*p < 0.05, one-way ANOVA with Tukey-Kramer post hoc test). On the other hand, regardless of dHAT CBP expression, the number of BRD4 spots did not change under KCl stimulation (p > 0.30, one-way ANOVA with Tukey-Kramer post hoc test). n = 17 cells in control neurons, n = 24 cells in dHAT CBP-expressing neurons, n = 21 cells in KCl-treated neurons, n = 18 cells in dHAT CBP-

expressing and KCl-treated neurons. (F) Representative images of H4ac signals in dHAT CBP-positive neurons. (G) The number of H4ac spots per cell in dHAT CBP-expressing neurons was significantly smaller than in control neurons (***p < 0.001, one-way ANOVA with Tukey-Kramer post hoc test). On the other hand, regardless of dHAT CBP expression, the number of H4ac spots did not change under KCl stimulation (p > 0.30, one-way ANOVA with Tukey-Kramer post hoc test). n = 17 cells in control neurons, n = 20 cells in dHAT CBP-expressing neurons, n = 16 cells in KCl-treated neurons, n = 19 cells in dHAT CBP-expressing and KCl-treated neurons. In (C and F), scale bar, 10 μm.

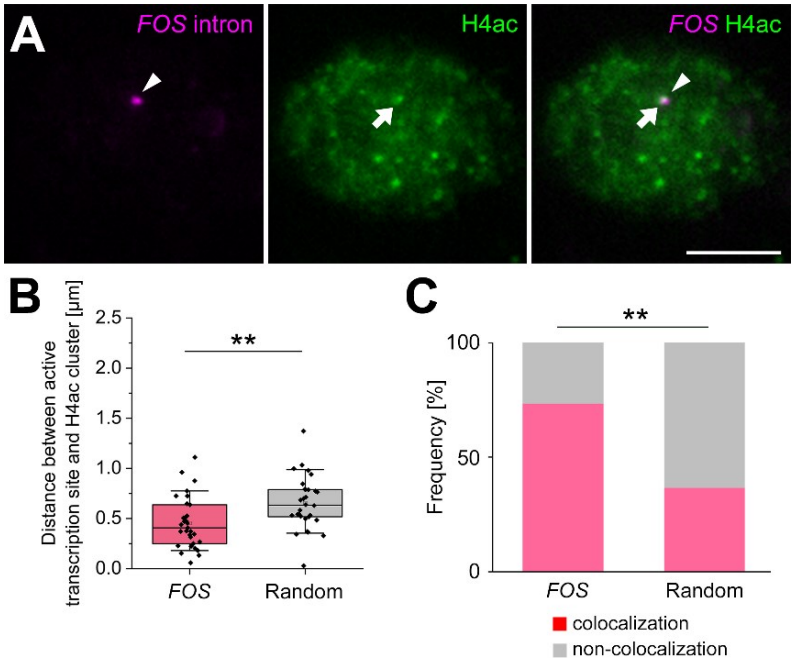

Figure 12. Activity-dependent gene transcription at histone H4-positive sites.

(A) Active transcription sites of *FOS* colocalized with H4ac spots (indicated by arrows) in 30 min KCl treatment. Active transcription sites were indicated by arrowheads. Scale bar, 5 μm. (B) Distances from *FOS* spots to the nearest H4ac spots were significantly smaller than those from randomized nuclear positions (**p < 0.01, Mann-Whitney U test). (C) The colocalization frequency between FOS and H4ac spots was significantly higher than the cases where the transcription sites were distributed randomly (**p < 0.01, Chi-square test). In (B and C), n= 30 alleles.

The influence of neuronal activity on formation of acetylation sites was also investigated, as neuronal activity has been reported to modify histone acetylation level of activity-dependent genes (Malik et al., 2014). Unexpectedly, the number of BRD4 spots was not changed by KCl treatment in control cells ($p = 0.70$, 50.5 ± 2.8 for KCl-, 46.4 ± 2.9 for KCl+, one-way ANOVA with Tukey Kramer test) as well as in dHAT CBP-expressing cells ($p = 0.052$, 29.3 ± 1.7 for KCl-, 38.7 ± 2.8 for KCl+, one-way ANOVA with Tukey Kramer test) (Figure 11C and D). The total BRD4 volume was not also altered by KCl treatment in both control and dHAT CBP-expressing cells (Figure 11E). Similar to BRD4, the number of H4ac spots was not changed by KCl treatment in both dHAT CBP-expressing cells ($p = 0.99$, 46.8 ± 2.4 for KCl-, 46.2 ± 2.5 for KCl+, one-way ANOVA with Tukey Kramer test) and control cells ($p = 0.30$, 30.3 ± 2.2 for KCl-, 36.6 ± 3.0 for KCl+, one-way ANOVA with Tukey Kramer test) (Figure 11F and G). These data indicate that histone acetylation sites and levels represented by BRD4 and H4ac are likely predetermined in the nuclei regardless of neuronal activity.

Since CBP HAT activity contributes to the formation of BRD4-positive acetylated sites and H4ac sites (Figure 11C-G), the effect of CBP HAT activity on CREB dynamics was also examined. To do this, the Tet-inducible HaloTag-CREB and EGFP-dHAT CBP expression vectors were co-transfected with pTα1-Dsred in cultured cells (Figure 13A and B). SMI showed that long residence CREB spots were markedly decreased in dHAT CBP-expressing neurons, while it was not affected by wild type CBP overexpression (Figure

13C). Quantitative analysis showed that A_2/A_1 was considerably smaller in dHAT CBP-expressing neurons than in control and wild type CBP-expressing neurons ($p < 0.01$, 0.23 ± 0.02 for control, 0.19 ± 0.02 for wild type CBP, 0.12 ± 0.03 for dHAT CBP, Kruskal-Wallis ANOVA with Dunn's post hoc test) (Table 4). As the frequency of long residence CREB spots was considerably decreased by dHAT CBP overexpression, the repetitive appearance of CREB spots was also inevitably suppressed. Thus, the formation of acetylated spots was reduced in the absence of CBP HAT activity, which may lead to disruption of CREB-CRE binding. On the other hand, wildtype CBP overexpression did not affect CREB-CRE binding, indicating that endogenous CBP expression is sufficient to generate histone acetylation sites for CREB-CRE binding.

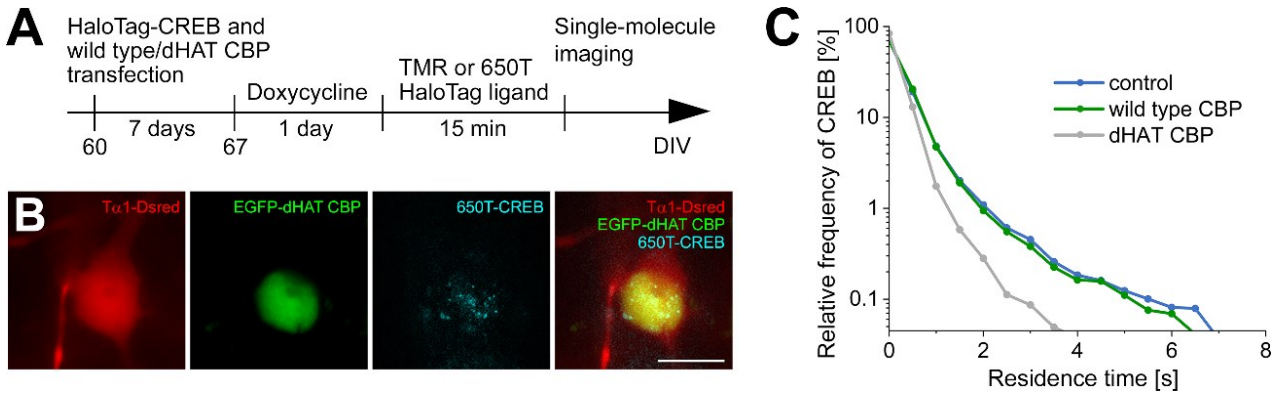

Figure 13. Disruption of CBP HAT activity inhibits CREB-CRE interaction.
(A) Experimental timeline of CREB SMI in dHAT CBP-expressing neurons. (B) Representative images of single-molecule CREB dynamics in Tα1-Dsred and EGFP-dHAT CBP expressing cells. Scale bar, 10 μm. (C) The residence time of CREB in dHAT CBP-expressing neurons was markedly shorter than that in EGFP-expressing neurons (***p = 1.1 x 10^{-8}, Kolmogorov-Smirnov test, n = 14 cells in control, n = 12 cells in dHAT CBP), while the residence time in wild type CBP-expressing neurons was not affected (p = 0.81, Kolmogorov-Smirnov test, n = 10 cells in wild type CBP).

	# of cells	# of cultures	t_1 [s]	t_2 [s]	A_2/A_1
control	14	3	0.33 ± 0.01	2.09 ± 0.20	0.23 ± 0.02
wild type CBP	10	3	0.34 ± 0.01	1.88 ± 0.13	0.19 ± 0.02
dHAT CBP	12	3	0.20 ± 0.03**	1.50 ± 0.32	0.12 ± 0.03**

Table 4. Dissociation rate constants and ratios of the long- to short-residence component of CREB spots in wild-type or mutant CBP-overexpressing cells.
Asterisks indicate that dissociation rate constant and the ratio of the long-residence to short-residence component of CREB in dHAT CBP-expressing cells were significantly different from that in control and wild-type CBP-expressing cells (**p<0.01, Kruskal-Wallis ANOVA with Dunn's post hoc test). The values represent mean ± SEM.

Neuronal activity promotes colocalization of CREB and CBP in the nucleus

To investigate an activity-dependent role of CBP in CREB-CRE binding, the direct interaction of CREB with CBP was investigated by simultaneous SMI of these molecules with different tags and fluorescent dyes (Joensuu et al., 2017; Niewidok et al., 2018). HaloTag-CREB and SNAPtag-CBP plasmids were co-transfected in cortical cells, and were visualized by TMR-conjugated HaloTag ligand and 647SiR-conjugated SNAPtag ligand, respectively (Figure 14A). CBP spot appearance was also expressed as the sum of two exponential curves with short- and long-time constants (see Equation 1). Based on the assumption that the long residence component represents specific interactions between CBP and other molecules, CBP spots with residence time longer than 0.6 s were selected for analysis (see Materials and Methods). As shown in Figure 14B, a CBP spot appeared overlapping with a long residence CREB spot during the observation. The colocalization was hardly detected under the resting condition, but the frequency of colocalization, which was defined as the ratio of the number of colocalized CREB spots to the total number of long residence CREB spots, was much enhanced by KCl treatment (0.2 ± 0.2% for KCl-, 4.2 ± 0.8% for KCl+, $p < 0.001$, Kruskal-Wallis ANOVA with Dunn's post hoc test) (Figure 14C).

In contrast, the colocalization frequency of CREB and SNAPtag alone (0.3 ± 0.2% for KCl+) was very low compared to SNAPtag-CBP under KCl stimulation, indicating that a non-specific binding property of SNAPtag does not affect the

result. Thus, it is likely that neuronal activity promotes CREB-CBP interactions at the single-molecule level.

The temporal features of these spots were further investigated. Interestingly, CREB spots tended to appear earlier than CBP spots. Quantitative analysis showed that long residence CREB spots emerged significantly earlier than colocalized CBP spots (0.5 ± 0.2 s, $p < 0.05$, one-sample t test against 0), although CREB and CBP spots disappeared at almost the same time (-0.2 ± 0.2 s, $p = 0.29$, one-sample t test against 0) (Figure 14D). This result suggests that CBP binding to CREB follows CREB-CRE binding.

Finally, I investigated the possibility that CBP binding to CREB is essential for CREB repetitive binding which leads to downstream gene expression. For this, cortical cells were transfected with the constitutively active CREB (CREB Y134F) which accelerates binding to CBP (Du et al., 2000; Suzuki et al., 2011). As shown in Figure 14E, the number of hotspots was significantly increased in CREB Y134F-expressing cells (0.4 ± 0.2 for wild type CREB, 1.8 ± 0.5 for phosphorylated CREB, $p < 0.05$, Mann-Whitney U test) without elevation of neuronal activity, suggesting that the interaction of CBP with activated CREB is essential for activity-dependent gene expression.

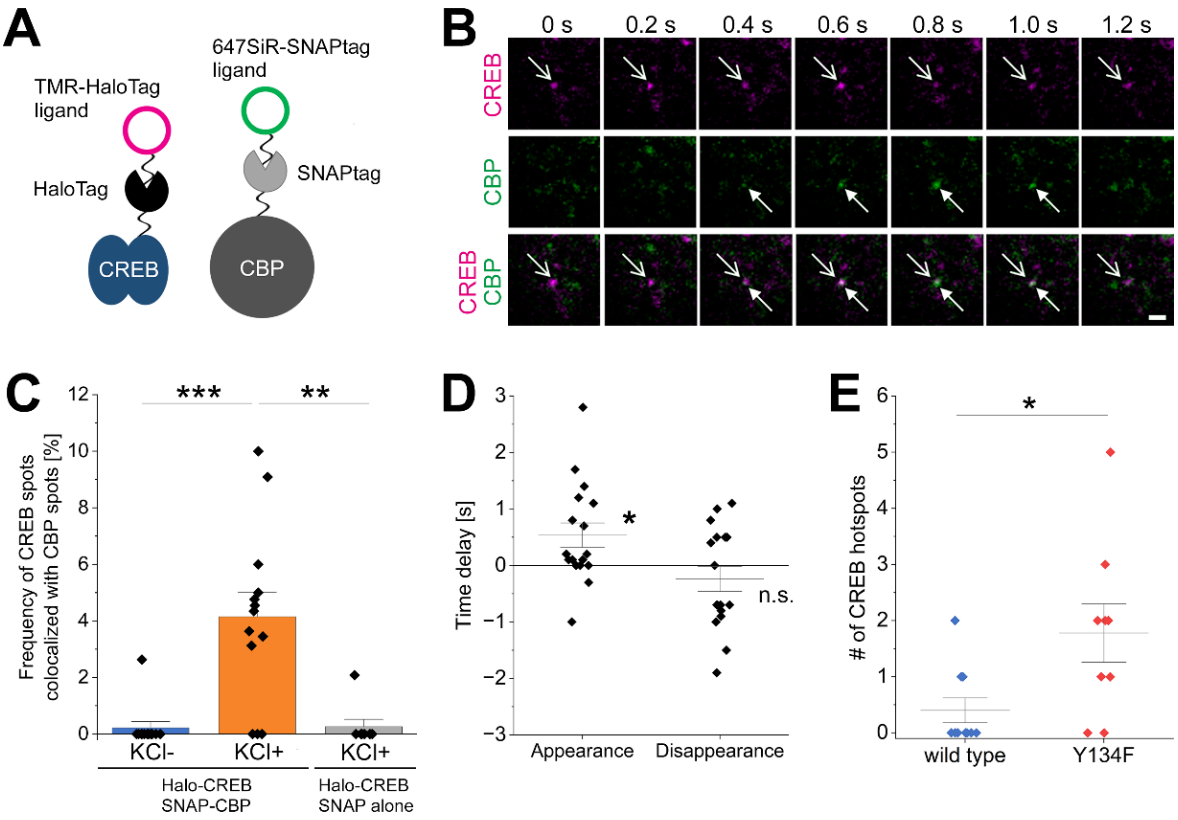

Figure 14. Activity-dependent CREB-CBP interaction at the single-molecule level.

(A) Schematic drawing of two-color SMI of HaloTag-CREB and SNAPtag-CBP. TMR-CREB and 647SiR-CBP were visualized simultaneously at the single-molecule level. (B) A CBP spot colocalized with a CREB spot in the nucleus. These two spots were indicated by white arrows. Scale bar, 1 μm. (C) The frequency of long residence CREB spots colocalized with CBP spots (> 0.6 s) was much increased by KCl treatment (***$p < 0.001$, Kruskal-Wallis ANOVA with Dunn's post hoc test) whereas the colocalization of CREB and SNAPtag alone was very low compared to SNAPtag-CBP under KCl stimulation (**$p < 0.01$, Kruskal-Wallis ANOVA with Dunn's post hoc test). n = 12 cells in KCl-, n = 13 cells in KCl+, n = 8 cells in SNAPtag alone KCl+. (D) Time delays of CBP binding to CREB (appearance) and CBP dissociation from CREB (disappearance) were measured (for 17 spots from 11 cells). CREB spots appearance was earlier than CBP spots (*$p<0.05$, one-sample t test against 0). (E) The number of CREB hotspots were compared between HaloTag-CREB

(wlid type) and CREB (Y134F). The number of CREB hotspots in Y134F was significantly higher than wild type (*p<0.05, Mann-Whitney U test, n = 9 cells for wild type, n = 9 cells for Y134F). The data of HaloTag-CREB (wild type) was used for Figure 7D.

Discussion

In this SMI study I demonstrated that the elevation of neuronal activity in human cortical neurons increased frequency of CREB-DNA and CREB-CBP interactions at fixed nuclear locations where activity-dependent gene expression is induced by active RNAPII. Evidence further demonstrated that repetitive CREB appearance and early response gene transcription occurred at BRD4- and H4ac-localized histone acetylation sites which were produced by CBP HAT activity prior to elevation of neuronal activity. Thus, these results support a model whereby neuronal activity-independent histone acetylation and activity-dependent CREB-DNA and CREB-CBP interactions contribute to regulating gene expression in response to neuronal activity.

Neuronal activity promotes repetitive CREB-DNA binding, leading to early response gene transcription

The present SMI demonstrated that neuronal activity increases repetitive CREB appearance at specific nuclear locations in human cortical neurons without changing the residence time distribution, in accordance with previous results in CREB dynamics in mouse cortical neurons (Kitagawa et al., 2017). Furthermore, RNAPII imaging strongly indicates that repetitive CREB binding to CRE promotes the active transcription of *FOS* and *NR4A1* through rapid RNAPII accumulation. One may think that the total time of CREB binding is more important. However, the fact that neuronal activity did not alter the kinetics of individual CREB molecules suggests that repetitive CREB binding to CRE

sites is indispensable for RNAPII accumulation and downstream gene expression. Consistent with this view, fluorescence recovery after photobleaching suggests that transcription factors frequently bind to DNA in response to stimulus signals (McNally et al., 2000; Rayasam et al., 2005; Sharp et al., 2006). On the other hand, individual binding time of serum response factor (SRF) has been reported to increase after stimulation (Hipp et al., 2019; Kuchler et al., 2022). There may be two possible modes of interaction between transcription factors and their target DNA for activity-dependent transcription.

Predetermined histone acetylation sites are scaffolds of activity-dependent transcription

It has been shown that histone acetylation sites represented by BRD4 spots are scattered in the nucleus of mouse ESCs (Sabari et al., 2018). The present imaging study further demonstrated that such acetylated sites are formed for activity-dependent gene expression in postmitotic neurons. I also found that a large population of these acetylated sites are produced by CBP HAT activity and scattered throughout the nucleus of cortical neurons, although CBP-independent HAT activity may also be involved (Figure 11D, E and G). Moreover, the fact that the number of histone acetylation sites was not changed with neuronal activation suggests that these acetylated sites are predetermined regardless of neuronal activity (Figure 11C-G). However, the possibility cannot be excluded that neuronal stimulation increases the histone acetylation level at some activity-dependent gene loci, since these acetylated sites should contain

not only activity-dependent but also cell type-specific gene loci (Malik et al., 2014; Tyssowski et al., 2018),(Kim et al., 2021). In addition, KCl treatment increased the colocalization of CREB and CBP (Figure 14C), suggesting the importance of neuronal activity-dependent CBP function at the predetermined sites. Neuronal activity has also shown to promote nucleocytoplasmic translocation of histone deacetylation enzymes and induce immediate early gene expression (Linseman et al., 2003; Sugo et al., 2010). Removal of deacetylation activity in the nucleus could contribute to appropriate activity-dependent gene expression together with local HAT activity.

The simultaneous measurement of CBP and CREB indicated that neuronal activity enhanced direct CREB-CBP interaction (Figure 14C). Given that CBP promotes RNAPII recruitment and elongation (Narita et al., 2021), it is conceivable that direct CBP binding to CREB induces downstream transcription via RNAPII accumulation. This view is also supported by the fact that CBP binding to CREB follows CREB-DNA binding (Figure 14D). In addition to RNAPII recruitment, activity-dependent CBP participation would further increase acetylation levels at predetermined acetylated loci, leading to repetitive CREB binding (Figure 14E) and subsequent RNA synthesis. Such activity-dependent CBP function might contribute to the selection of specific gene loci from a large number of acetylation sites.

Biochemical studies have demonstrated that neuronal activity induces rapid CREB phosphorylation in the nucleus (Hardingham et al., 2001; Greer and Greenberg, 2008), resulting in recruitment of RNAPII by CBP (Mayr and

Montminy, 2001; Lonze and Ginty, 2002; Narita et al., 2021). The present findings would add the following scenario to the activity-dependent transcription mechanism in terms of spatiotemporal regulation. 1) In the absence of electrical activity, predetermined histone acetylation sites are scattered throughout the nucleus to prepare for transcription of activity-dependent genes. 2) Neuronal activity promotes CBP-CREB interaction and repetitive CREB-CRE binding at the predetermined gene loci. 3) Finally, rapid RNAPII accumulation is induced, and mRNA synthesis of activity-dependent genes such as *FOS* and *NR4A1* is accelerated. I would like to emphasize that histone acetylation predetermined by CBP HAT activity and neuronal activity-dependent CREB-CRE and CBP-CREB binding regulate rapid transcription of specific genes.

Dysregulation of CREB dynamics may be relevant to neurological pathology

In the present study, I demonstrate that inactivation of CBP HAT leads to disruption of activity-dependent CREB dynamics in human cortical neurons, which could be directly relevant to the disease mechanisms found in Rubinstein-Taybi syndrome or in mouse models. Consistent with this view, iPSC-derived neurons from Rubinstein-Taybi syndrome patients have shown impaired neurite outgrowth (Alari et al., 2018; Alari et al., 2021). Abnormalities of gene expression and cognitive functions have also been reported in CBP mutant mice (Wood et al., 2005; Vieira and Korzus, 2015).

In accordance with the previous study using mouse cortical neurons

(Kitagawa et al., 2017), the present study demonstrated that neuronal activity also promotes repetitive CREB-CRE binding in human cortical neurons, suggesting that activity-dependent CREB dynamics is shared across species. However, CREB-CRE binding time (t_2) was shorter in human cortical neurons (compare Tables S2 and S3 in this study with Tables 2 and 3 in the reference paper) (Kitagawa et al., 2017). This might enable precise gene regulation in human cortical neurons by increasing the temporal resolution. A recent study suggests that human genomic regions showing dynamic changes in human lineage regulate the expression of neurodevelopmental genes (Girskis et al., 2021). Another genome-wide analysis reported human-specific histone methylation patterns in neuropsychiatric disease-associated genes (Shulha et al., 2012). These evolutionary genomic and chromatin structural changes around CRE sequences might contribute to generating the difference in CREB-CRE binding time between human and mouse cortical neurons. Furthermore, as previous studies have demonstrated that neuronal maturation and biochemical reactions including transcription are slower in human (Stewart-Ornstein et al., 2017; Matsuda et al., 2020; Iwata et al., 2023), it would be interesting whether other temporal aspects in activity-dependent transcription are involved in plasticity of human cortical neurons.

Limitation of study

The present results demonstrated the spatiotemporal dynamics of the transcription factors and the histone-modifying enzymes by carefully analyzing the nuclear locations of these molecules, and delineated the specific localization of CREB and its colocalization with RNAPII, BRD4, and activity-dependent transcripts. Yet, this does not mean that these molecules bind and/or interact directly with each other. However, present findings strongly suggest that these molecules are assembled in a spatiotemporal manner. This approach would give an insight into the molecular mechanisms that have not been elucidated by conventional biochemical and molecular biological studies.

The present study did not directly visualize any CRE sites in the nucleus, but the results in the mutant CREB and cell-free conditions strongly suggest that CREB binds to CRE sites in the genome of human cortical cells. The fact that RNAPII accumulation and activity-dependent gene transcription occurred at CREB hotspots further supports this view.

I also utilized human ESC-derived cortical neurons to investigate the dynamics of transcription factors and chromatin modifiers. One problem is that cell sampling is biased toward deep-layer neurons rather than upper-layer neurons. Indeed, most cells in the culture condition were CTIP2- or TBR1-positive neurons. Furthermore, these cells may not yet be fully differentiated. It is likely that the extent of neuronal maturation affected activity-dependent responsiveness. As described above, roughly 14 % of cells did not express phosphorylated CREB in KCl treatment, indicating that these cells were unable

to respond to neuronal activity (Figure 2A). The fact that a small population of cells did show neither hotspots nor colocalization of CREB with CBP even with neuronal stimulation may be due to the inactive state of CREB (Figure 6F, 7D and 14E). Therefore, more plastic aspects in cortical neurons may be obtained by combining an organoid technique, which could lead to important findings to reveal gene regulation mechanisms of cortical plasticity and neuronal diseases.

References

Alari V, Scalmani P, Ajmone PF, Perego S, Avignone S, Catusi I, Lonati PA, Borghi MO, Finelli P, Terragni B, Mantegazza M, Russo S, Larizza L (2021) Histone Deacetylase Inhibitors Ameliorate Morphological Defects and Hypoexcitability of iPSC-Neurons from Rubinstein-Taybi Patients. Int J Mol Sci 22.

Alari V, Russo S, Terragni B, Ajmone PF, Sironi A, Catusi I, Calzari L, Concolino D, Marotta R, Milani D, Giardino D, Mantegazza M, Gervasini C, Finelli P, Larizza L (2018) iPSC-derived neurons of CREBBP- and EP300-mutated Rubinstein-Taybi syndrome patients show morphological alterations and hypoexcitability. Stem Cell Res 30:130-140.

Amir RE, Van den Veyver IB, Wan M, Tran CQ, Francke U, Zoghbi HY (1999) Rett syndrome is caused by mutations in X-linked MECP2, encoding methyl-CpG-binding protein 2. Nat Genet 23:185-188.

Bading H, Ginty DD, Greenberg ME (1993) Regulation of gene expression in hippocampal neurons by distinct calcium signaling pathways. Science 260:181-186.

Bannister AJ, Kouzarides T (1996) The CBP co-activator is a histone acetyltransferase. Nature 384:641-643.

Bito H, Deisseroth K, Tsien RW (1996) CREB phosphorylation and dephosphorylation: a Ca(2+)- and stimulus duration-dependent switch for hippocampal gene expression. Cell 87:1203-1214.

Boulting GL, Durresi E, Ataman B, Sherman MA, Mei K, Harmin DA, Carter AC, Hochbaum DR, Granger AJ, Engreitz JM, Hrvatin S, Blanchard MR, Yang MG, Griffith EC, Greenberg ME (2021) Activity-dependent regulome of human GABAergic neurons reveals new patterns of gene regulation and neurological disease heritability. Nat Neurosci 24:437-448.

Buratowski S (2009) Progression through the RNA polymerase II CTD cycle. Mol Cell 36:541-546.

Chen J, Zhang Z, Li L, Chen BC, Revyakin A, Hajj B, Legant W, Dahan M, Lionnet T, Betzig E, Tjian R, Liu Z (2014) Single-molecule dynamics of enhanceosome assembly in embryonic stem cells. Cell 156:1274-1285.

Chen LF, Lin YT, Gallegos DA, Hazlett MF, Gomez-Schiavon M, Yang MG, Kalmeta B, Zhou AS, Holtzman L, Gersbach CA, Grandl J, Buchler NE, West AE (2019) Enhancer Histone Acetylation Modulates Transcriptional Bursting Dynamics of

Neuronal Activity-Inducible Genes. Cell Rep 26:1174-1188 e1175.

Chrivia JC, Kwok RP, Lamb N, Hagiwara M, Montminy MR, Goodman RH (1993) Phosphorylated CREB binds specifically to the nuclear protein CBP. Nature 365:855-859.

Cook PR (1999) The organization of replication and transcription. Science 284:1790-1795.

Du K, Asahara H, Jhala US, Wagner BL, Montminy M (2000) Characterization of a CREB gain-of-function mutant with constitutive transcriptional activity in vivo. Mol Cell Biol 20:4320-4327.

Ebert DH, Greenberg ME (2013) Activity-dependent neuronal signalling and autism spectrum disorder. Nature 493:327-337.

Espuny-Camacho I, Michelsen KA, Gall D, Linaro D, Hasche A, Bonnefont J, Bali C, Orduz D, Bilheu A, Herpoel A, Lambert N, Gaspard N, Peron S, Schiffmann SN, Giugliano M, Gaillard A, Vanderhaeghen P (2013) Pyramidal neurons derived from human pluripotent stem cells integrate efficiently into mouse brain circuits in vivo. Neuron 77:440-456.

Esvald EE, Tuvikene J, Sirp A, Patil S, Bramham CR, Timmusk T (2020) CREB Family Transcription Factors Are Major Mediators of BDNF Transcriptional Autoregulation in Cortical Neurons. J Neurosci 40:1405-1426.

Filippakopoulos P, Picaud S, Mangos M, Keates T, Lambert JP, Barsyte-Lovejoy D, Felletar I, Volkmer R, Muller S, Pawson T, Gingras AC, Arrowsmith CH, Knapp S (2012) Histone recognition and large-scale structural analysis of the human bromodomain family. Cell 149:214-231.

Fowler T, Sen R, Roy AL (2011) Regulation of primary response genes. Mol Cell 44:348-360.

Girskis KM et al. (2021) Rewiring of human neurodevelopmental gene regulatory programs by human accelerated regions. Neuron 109:3239-3251 e3237.

Gong F, Chiu LY, Cox B, Aymard F, Clouaire T, Leung JW, Cammarata M, Perez M, Agarwal P, Brodbelt JS, Legube G, Miller KM (2015) Screen identifies bromodomain protein ZMYND8 in chromatin recognition of transcription-associated DNA damage that promotes homologous recombination. Genes Dev 29:197-211.

Greer PL, Greenberg ME (2008) From synapse to nucleus: calcium-dependent gene transcription in the control of synapse development and function. Neuron 59:846-860.

Hardingham GE, Arnold FJ, Bading H (2001) Nuclear calcium signaling controls CREB-

mediated gene expression triggered by synaptic activity. Nat Neurosci 4:261-267.
Hatanaka Y, Murakami F (2002) In vitro analysis of the origin, migratory behavior, and maturation of cortical pyramidal cells. J Comp Neurol 454:1-14.
Hipp L, Beer J, Kuchler O, Reisser M, Sinske D, Michaelis J, Gebhardt JCM, Knoll B (2019) Single-molecule imaging of the transcription factor SRF reveals prolonged chromatin-binding kinetics upon cell stimulation. Proc Natl Acad Sci U S A 116:880-889.
Impey S, Fong AL, Wang Y, Cardinaux JR, Fass DM, Obrietan K, Wayman GA, Storm DR, Soderling TR, Goodman RH (2002) Phosphorylation of CBP mediates transcriptional activation by neural activity and CaM kinase IV. Neuron 34:235-244.
Iwata R et al. (2023) Mitochondria metabolism sets the species-specific tempo of neuronal development. Science 379:eabn4705.
Joensuu M, Martínez-Mármol R, Padmanabhan P, Glass NR, Durisic N, Pelekanos M, Mollazade M, Balistreri G, Amor R, Cooper-White JJ, Goodhill GJ, Meunier FA (2017) Visualizing endocytic recycling and trafficking in live neurons by subdiffractional tracking of internalized molecules. Nat Protoc 12:2590-2622.
Joo JY, Schaukowitch K, Farbiak L, Kilaru G, Kim TK (2016) Stimulus-specific combinatorial functionality of neuronal c-fos enhancers. Nat Neurosci 19:75-83.
Kaplan L, Ierokomos A, Chowdary P, Bryant Z, Cui B (2018) Rotation of endosomes demonstrates coordination of molecular motors during axonal transport. Sci Adv 4:e1602170.
Kim SK, Liu X, Park J, Um D, Kilaru G, Chiang CM, Kang M, Huber KM, Kang K, Kim TK (2021) Functional coordination of BET family proteins underlies altered transcription associated with memory impairment in fragile X syndrome. Sci Adv 7.
Kim TK, Hemberg M, Gray JM, Costa AM, Bear DM, Wu J, Harmin DA, Laptewicz M, Barbara-Haley K, Kuersten S, Markenscoff-Papadimitriou E, Kuhl D, Bito H, Worley PF, Kreiman G, Greenberg ME (2010) Widespread transcription at neuronal activity-regulated enhancers. Nature 465:182-187.
Kitagawa H, Sugo N, Morimatsu M, Arai Y, Yanagida T, Yamamoto N (2017) Activity-Dependent Dynamics of the Transcription Factor of cAMP-Response Element Binding Protein in Cortical Neurons Revealed by Single-Molecule Imaging. J Neurosci 37:1-10.
Kornhauser JM, Cowan CW, Shaywitz AJ, Dolmetsch RE, Griffith EC, Hu LS, Haddad C, Xia Z, Greenberg ME (2002) CREB transcriptional activity in neurons is

regulated by multiple, calcium-specific phosphorylation events. Neuron 34:221-233.

Korzus E (2017) Rubinstein-Taybi Syndrome and Epigenetic Alterations. Adv Exp Med Biol 978:39-62.

Korzus E, Rosenfeld MG, Mayford M (2004) CBP histone acetyltransferase activity is a critical component of memory consolidation. Neuron 42:961-972.

Kuchler O, Gerlach J, Vomhof T, Hettich J, Steinmetz J, Gebhardt JCM, Michaelis J, Knoll B (2022) Single-molecule tracking (SMT) and localization of SRF and MRTF transcription factors during neuronal stimulation and differentiation. Open Biol 12:210383.

Li J, Dong A, Saydaminova K, Chang H, Wang G, Ochiai H, Yamamoto T, Pertsinidis A (2019) Single-Molecule Nanoscopy Elucidates RNA Polymerase II Transcription at Single Genes in Live Cells. Cell 178:491-506 e428.

Linaro D, Vermaercke B, Iwata R, Ramaswamy A, Libe-Philippot B, Boubakar L, Davis BA, Wierda K, Davie K, Poovathingal S, Penttila PA, Bilheu A, De Bruyne L, Gall D, Conzelmann KK, Bonin V, Vanderhaeghen P (2019) Xenotransplanted Human Cortical Neurons Reveal Species-Specific Development and Functional Integration into Mouse Visual Circuits. Neuron 104:972-986 e976.

Linseman DA, Bartley CM, Le SS, Laessig TA, Bouchard RJ, Meintzer MK, Li M, Heidenreich KA (2003) Inactivation of the myocyte enhancer factor-2 repressor histone deacetylase-5 by endogenous Ca(2+) //calmodulin-dependent kinase II promotes depolarization-mediated cerebellar granule neuron survival. J Biol Chem 278:41472-41481.

Liu Z, Legant WR, Chen BC, Li L, Grimm JB, Lavis LD, Betzig E, Tjian R (2014) 3D imaging of Sox2 enhancer clusters in embryonic stem cells. Elife 3:e04236.

Lonze BE, Ginty DD (2002) Function and regulation of CREB family transcription factors in the nervous system. Neuron 35:605-623.

Loven J, Hoke HA, Lin CY, Lau A, Orlando DA, Vakoc CR, Bradner JE, Lee TI, Young RA (2013) Selective inhibition of tumor oncogenes by disruption of super-enhancers. Cell 153:320-334.

Malik AN, Vierbuchen T, Hemberg M, Rubin AA, Ling E, Couch CH, Stroud H, Spiegel I, Farh KK, Harmin DA, Greenberg ME (2014) Genome-wide identification and characterization of functional neuronal activity-dependent enhancers. Nat Neurosci 17:1330-1339.

Malyshevskaya O, Shiraishi Y, Kimura F, Yamamoto N (2013) Role of electrical activity in horizontal axon growth in the developing cortex: a time-lapse study using

optogenetic stimulation. PLoS One 8:e82954.

Marmorstein R, Zhou MM (2014) Writers and readers of histone acetylation: structure, mechanism, and inhibition. Cold Spring Harb Perspect Biol 6:a018762.

Matsuda M, Hayashi H, Garcia-Ojalvo J, Yoshioka-Kobayashi K, Kageyama R, Yamanaka Y, Ikeya M, Toguchida J, Alev C, Ebisuya M (2020) Species-specific segmentation clock periods are due to differential biochemical reaction speeds. Science 369:1450-1455.

Mayr B, Montminy M (2001) Transcriptional regulation by the phosphorylation-dependent factor CREB. Nat Rev Mol Cell Biol 2:599-609.

McNally JG, Müller WG, Walker D, Wolford R, Hager GL (2000) The glucocorticoid receptor: rapid exchange with regulatory sites in living cells. Science 287:1262-1265.

Miyasaka Y, Yamamoto N (2021) Neuronal Activity Patterns Regulate Brain-Derived Neurotrophic Factor Expression in Cortical Cells via Neuronal Circuits. Front Neurosci 15:699583.

Narita T, Ito S, Higashijima Y, Chu WK, Neumann K, Walter J, Satpathy S, Liebner T, Hamilton WB, Maskey E, Prus G, Shibata M, Iesmantavicius V, Brickman JM, Anastassiadis K, Koseki H, Choudhary C (2021) Enhancers are activated by p300/CBP activity-dependent PIC assembly, RNAPII recruitment, and pause release. Mol Cell 81:2166-2182 e2166.

Niewidok B, Igaev M, Pereira da Graca A, Strassner A, Lenzen C, Richter CP, Piehler J, Kurre R, Brandt R (2018) Single-molecule imaging reveals dynamic biphasic partition of RNA-binding proteins in stress granules. J Cell Biol 217:1303-1318.

Nozaki T, Imai R, Tanbo M, Nagashima R, Tamura S, Tani T, Joti Y, Tomita M, Hibino K, Kanemaki MT, Wendt KS, Okada Y, Nagai T, Maeshima K (2017) Dynamic Organization of Chromatin Domains Revealed by Super-Resolution Live-Cell Imaging. Mol Cell 67:282-293.e287.

Ohishi H, Shimada S, Uchino S, Li J, Sato Y, Shintani M, Owada H, Ohkawa Y, Pertsinidis A, Yamamoto T, Kimura H, Ochiai H (2022) STREAMING-tag system reveals spatiotemporal relationships between transcriptional regulatory factors and transcriptional activity. Nat Commun 13:7672.

Petrij F, Giles RH, Dauwerse HG, Saris JJ, Hennekam RC, Masuno M, Tommerup N, van Ommen GJ, Goodman RH, Peters DJ, et al. (1995) Rubinstein-Taybi syndrome caused by mutations in the transcriptional co-activator CBP. Nature 376:348-351.

Pumo GM, Kitazawa T, Rijli FM (2022) Epigenetic and Transcriptional Regulation of Spontaneous and Sensory Activity Dependent Programs During Neuronal Circuit

Development. Front Neural Circuits 16:911023.

Rayasam GV, Elbi C, Walker DA, Wolford R, Fletcher TM, Edwards DP, Hager GL (2005) Ligand-specific dynamics of the progesterone receptor in living cells and during chromatin remodeling in vitro. Mol Cell Biol 25:2406-2418.

Renner M, Wang L, Levi S, Hennekinne L, Triller A (2017) A Simple and Powerful Analysis of Lateral Subdiffusion Using Single Particle Tracking. Biophys J 113:2452-2463.

Sabari BR et al. (2018) Coactivator condensation at super-enhancers links phase separation and gene control. Science 361.

Sharp ZD, Mancini MG, Hinojos CA, Dai F, Berno V, Szafran AT, Smith KP, Lele TP, Ingber DE, Mancini MA (2006) Estrogen-receptor-alpha exchange and chromatin dynamics are ligand- and domain-dependent. J Cell Sci 119:4101-4116.

Shi Y, Kirwan P, Smith J, Robinson HP, Livesey FJ (2012) Human cerebral cortex development from pluripotent stem cells to functional excitatory synapses. Nat Neurosci 15:477-486, S471.

Shulha HP, Crisci JL, Reshetov D, Tushir JS, Cheung I, Bharadwaj R, Chou HJ, Houston IB, Peter CJ, Mitchell AC, Yao WD, Myers RH, Chen JF, Preuss TM, Rogaev EI, Jensen JD, Weng Z, Akbarian S (2012) Human-specific histone methylation signatures at transcription start sites in prefrontal neurons. PLoS Biol 10:e1001427.

Specht CG, Izeddin I, Rodriguez PC, El Beheiry M, Rostaing P, Darzacq X, Dahan M, Triller A (2013) Quantitative nanoscopy of inhibitory synapses: counting gephyrin molecules and receptor binding sites. Neuron 79:308-321.

Speil J, Baumgart E, Siebrasse JP, Veith R, Vinkemeier U, Kubitscheck U (2011) Activated STAT1 transcription factors conduct distinct saltatory movements in the cell nucleus. Biophys J 101:2592-2600.

Spena S, Milani D, Rusconi D, Negri G, Colapietro P, Elcioglu N, Bedeschi F, Pilotta A, Spaccini L, Ficcadenti A, Magnani C, Scarano G, Selicorni A, Larizza L, Gervasini C (2015) Insights into genotype-phenotype correlations from CREBBP point mutation screening in a cohort of 46 Rubinstein-Taybi syndrome patients. Clin Genet 88:431-440.

Stewart-Ornstein J, Cheng HWJ, Lahav G (2017) Conservation and Divergence of p53 Oscillation Dynamics across Species. Cell Syst 5:410-417 e414.

Sugo N, Oshiro H, Takemura M, Kobayashi T, Kohno Y, Uesaka N, Song WJ, Yamamoto N (2010) Nucleocytoplasmic translocation of HDAC9 regulates gene expression and dendritic growth in developing cortical neurons. Eur J Neurosci 31:1521-1532.

Sugo N, Morimatsu M, Arai Y, Kousoku Y, Ohkuni A, Nomura T, Yanagida T, Yamamoto N (2015) Single-Molecule Imaging Reveals Dynamics of CREB Transcription Factor Bound to Its Target Sequence. Sci Rep 5:10662.

Suzuki A, Fukushima H, Mukawa T, Toyoda H, Wu LJ, Zhao MG, Xu H, Shang Y, Endoh K, Iwamoto T, Mamiya N, Okano E, Hasegawa S, Mercaldo V, Zhang Y, Maeda R, Ohta M, Josselyn SA, Zhuo M, Kida S (2011) Upregulation of CREB-mediated transcription enhances both short- and long-term memory. J Neurosci 31:8786-8802.

Thompson A, Gribizis A, Chen C, Crair MC (2017) Activity-dependent development of visual receptive fields. Curr Opin Neurobiol 42:136-143.

Tokunaga M, Imamoto N, Sakata-Sogawa K (2008) Highly inclined thin illumination enables clear single-molecule imaging in cells. Nat Methods 5:159-161.

Tyssowski KM, DeStefino NR, Cho JH, Dunn CJ, Poston RG, Carty CE, Jones RD, Chang SM, Romeo P, Wurzelmann MK, Ward JM, Andermann ML, Saha RN, Dudek SM, Gray JM (2018) Different Neuronal Activity Patterns Induce Different Gene Expression Programs. Neuron 98:530-546 e511.

Uchino S, Ito Y, Sato Y, Handa T, Ohkawa Y, Tokunaga M, Kimura H (2022) Live imaging of transcription sites using an elongating RNA polymerase II-specific probe. J Cell Biol 221.

Vieira PA, Korzus E (2015) CBP-Dependent memory consolidation in the prefrontal cortex supports object-location learning. Hippocampus 25:1532-1540.

Walton KM, Rehfuss RP, Chrivia JC, Lochner JE, Goodman RH (1992) A dominant repressor of cyclic adenosine 3',5'-monophosphate (cAMP)-regulated enhancer-binding protein activity inhibits the cAMP-mediated induction of the somatostatin promoter in vivo. Mol Endocrinol 6:647-655.

West AE, Greenberg ME (2011) Neuronal activity-regulated gene transcription in synapse development and cognitive function. Cold Spring Harb Perspect Biol 3.

Wood MA, Kaplan MP, Park A, Blanchard EJ, Oliveira AM, Lombardi TL, Abel T (2005) Transgenic mice expressing a truncated form of CREB-binding protein (CBP) exhibit deficits in hippocampal synaptic plasticity and memory storage. Learn Mem 12:111-119.

Yamamoto N, López-Bendito G (2012) Shaping brain connections through spontaneous neural activity. Eur J Neurosci 35:1595-1604.

Yamamoto N, Okada Y (2020) Single Molecule Microscopy in Neurobiology: Springer.

Yao J, Ardehali MB, Fecko CJ, Webb WW, Lis JT (2007) Intranuclear distribution and local dynamics of RNA polymerase II during transcription activation. Mol Cell

28:978-990.

Zhan H, Stanciauskas R, Stigloher C, Keomanee-Dizon K, Jospin M, Bessereau JL, Pinaud F (2014) In vivo single-molecule imaging identifies altered dynamics of calcium channels in dystrophin-mutant C. elegans. Nat Commun 5:4974.

Zhang X, Odom DT, Koo SH, Conkright MD, Canettieri G, Best J, Chen H, Jenner R, Herbolsheimer E, Jacobsen E, Kadam S, Ecker JR, Emerson B, Hogenesch JB, Unterman T, Young RA, Montminy M (2005) Genome-wide analysis of cAMP-response element binding protein occupancy, phosphorylation, and target gene activation in human tissues. Proc Natl Acad Sci U S A 102:4459-4464.

Acknowledgement

I am really grateful to Drs. Nobuhiko Yamamoto and Noriyuki Sugo for supervising and supporting overall this study. They always supervised me the experiments, how to progress the research, writing a paper. I also thank Dr. Takeshi Yagi for critical reading and continuous encouragement. Drs. Ryuichi Shirasaki and Yumiko Hatanaka gave me so many advices at laboratory seminar, so I appreciate him for nice suggestions. I appreciate that Drs. Tetsuro Hirose, Takeo Horie and Akihiko Ishijima kindly accepted my committee members and gave me useful suggestions. Finally, I am so grateful to Yamamoto-lab and Yagi-lab members for helpful comments and discussions on my research.

Papers and conference presentations related to this thesis

(1) Publication

Atsumi Y, Iwata R, Kimura H, Vanderhaeghen P, Yamamoto N and Sugo N. Repetitive CREB-DNA interactions at gene loci predetermined by CBP induce activity-dependent gene expression in human cortical neurons. ***Cell Reports***, 113576 (online), 2023.

(2) Conference presentations

Atsumi Y, Iwata R, Kimura H, Vanderhaeghen P, Sugo N and Yamamoto N. ヒト大脳皮質神経細胞の神経活動依存的な転写はヒストンアセチル化によって決められた遺伝子座に転写調節因子 CREB が繰り返し結合することで引き起こされる. ポスター番号 2P-160, 第 46 回日本分子生物学会（神戸）, 2023 年 12 月

Atsumi Y, Iwata R, Kimura H, Vanderhaeghen P, Sugo N and Yamamoto N. ヒト神経細胞の活動依存的転写は転写調節因子 CREB がヒストンアセチル化酵素 CBP で決定された標的遺伝子に繰り返し結合することで促進される. 演題番号 1GD1600, 第 61 回日本生物物理学会（名古屋）, 2023 年 11 月

Atsumi Y, Iwata R, Kimura H, Vanderhaeghen P, Sugo N and Yamamoto N. Spatiotemporal dynamics of CREB with cofactors regulate activity-dependent gene expression in human cortical neurons. Development and Plasticity of the

Brain（伊勢志摩）, 2022 年 10 月

Atsumi Y, Iwata R, Kimura H, Vanderhaeghen P, Sugo N and Yamamoto N. ヒト由来大脳皮質ニューロンにおいて CREB と共因子の時空間的な動態が神経活動依存的な遺伝子発現を制御する. 若手道場, 第 45 回日本神経科学大会（沖縄宜野湾）, 2022 年 7 月

Atsumi Y, Iwata R, Kimura H, Vanderhaeghen P, Sugo N and Yamamoto N. ヒト由来大脳皮質神経細胞において共因子を伴った CREB の動態変化が神経活動依存的に転写を促進する. 第 15 回神経発生討論会（オンライン）, 2022 年 3 月

Atsumi Y, Iwata R, Vanderhaeghen P, Sugo N and Yamamoto N. Activity-dependent dynamics of the transcription factor CREB via cofactor CBP in human cortical-like neurons. 第 43 回神経組織培養研究会（オンライン）, 2021 年 11 月

Atsumi Y, Iwata R, Vanderhaeghen P, Sugo N and Yamamoto N.ヒト由来大脳皮質神経細胞における転写調節因子 CREB の共因子 CBP を介した神経活動依存的な動態変化. 演題番号 C000872, 第 44 回日本神経科学大会（神戸）, 2021 年 7 月

Atsumi Y, Iwata R, Vanderhaeghen P, Sugo N and Yamamoto N. Dynamics of the transcription factor CREB through CBP binding in human cortical-like neurons: A study using single-molecule imaging. The NIG Symposium 2020（オンライン）, 2020 年 12 月

Atsumi Y, Iwata R, Vanderhaeghen P, Sugo N and Yamamoto N. ヒト由来大脳皮質ニューロンにおける神経活動依存的な転写調節因子 CREB の動態：１分子イメージングによる解析. ポスター番号 P1-1-05, 新学術領域研究 スクラップ&ビルドによる脳機能の動的制御 第 5 回領域会議（オンライン）, 2020 年 8 月

Atsumi Y, Iwata R, Vanderhaeghen P, Sugo N and Yamamoto N. Activity-dependent dynamics of the transcription factor CREB in human cortical-like neurons: A study using single-molecule imaging. Lecture 3603, Federation of European Neuroscience Societies, FENS（オンライン）, 2020 年 7 月

Atsumi Y, Iwata R, Vanderhaeghen P, Sugo N and Yamamoto N. ヒト由来大脳皮質神経細胞における神経活動依存的な転写調節因子 CREB の 1 分子イメージング. 演題番号 4301000052, 第 43 回日本神経科学大会（オンライン）, 2020 年 7 月

Atsumi Y, Iwata R, Vanderhaeghen P, Sugo N and Yamamoto N. Single-molecule imaging of CREB transcription factor in human cortical-like neurons. P11.27, International Brain Research Organization, IBRO（韓国大邱）, 2019 年

9 月